Innovations Deserving
Exploratory Analysis Programs

Highway IDEA Program

Development of a Simple Test to Determine the Low Temperature Strength of Asphalt Mixtures and Binders

Final Report for
Highway IDEA Project 151

Prepared by:
Mihai Marasteanu, Augusto Cannone Falchetto, Mugurel Turos, Jia-Liang Le
University of Minnesota

December 2012

TRANSPORTATION RESEARCH BOARD
OF THE NATIONAL ACADEMIES

Innovations Deserving Exploratory Analysis (IDEA) Programs
Managed by the Transportation Research Board

This IDEA project was funded by the NCHRP IDEA Program.

The TRB currently manages the following three IDEA programs:

- The NCHRP IDEA Program, which focuses on advances in the design, construction, and maintenance of highway systems, is funded by American Association of State Highway and Transportation Officials (AASHTO) as part of the National Cooperative Highway Research Program (NCHRP).
- The Safety IDEA Program currently focuses on innovative approaches for improving railroad safety or performance. The program is currently funded by the Federal Railroad Administration (FRA). The program was previously jointly funded by the Federal Motor Carrier Safety Administration (FMCSA) and the FRA.
- The Transit IDEA Program, which supports development and testing of innovative concepts and methods for advancing transit practice, is funded by the Federal Transit Administration (FTA) as part of the Transit Cooperative Research Program (TCRP).

Management of the three IDEA programs is coordinated to promote the development and testing of innovative concepts, methods, and technologies.

For information on the IDEA programs, check the IDEA website (www.trb.org/idea). For questions, contact the IDEA programs office by telephone at (202) 334-3310.

IDEA Programs
Transportation Research Board
500 Fifth Street, NW
Washington, DC 20001

Development of a Simple Test to Determine the Low Temperature Strength of Asphalt Mixtures and Binders

IDEA Program Final Report

NCHRP IDEA 151

Prepared for the IDEA Program

Transportation Research Board

The National Academies

Mihai Marasteanu
Augusto Cannone Falchetto
Mugurel Turos
Jia-Liang Le

University of Minnesota

December 2012

TABLE OF CONTENTS

LIST OF TABLES

LIST OF FIGURES

ACKNOWLEDGEMENTS

The authors would like to acknowledge the assistance provided by the expert panel during this project: Kevin Van Frank, Utah Department of Transportation; Maureen Jensen, Minnesota Department of Transportation; and Chuck Maggi, Cannon Instrument Company.

The authors would like to thank David Kilpatrick, Connecticut Department of Transportation, for his contribution as the research advisor in this IDEA investigation.

Special recognition goes to Dr. Inam Jawed for his support and guidance during the entire duration of this project.

EXECUTIVE SUMMARY

The idea of performing strength tests at low temperature on asphalt mixture and asphalt binder beam specimens with the Bending Beam Rheometer (BBR) is investigated in this project. The first part of this report provides a review of the theory of strength size effect for quasibrittle materials. This section includes energetic-statistic size effect, weakest link model (WLM) and Weibull statistics. The theory is then used in the analysis part of the research to evaluate and extrapolate the experimental results and to compare the results obtained with different strength tests.

In the second part, the exploratory experimental investigation initially performed is first presented. Preliminary strength results obtained on BBR asphalt mixture beams are discussed and BBR strength results are compared with the current Indirect Tensile Test (IDT) strength method. The results of similar experimental work used to obtain asphalt binder BBR strength are then discussed and compared with the current Direct Tension Test (DTT) strength testing method.

Based on this initial experimental work, a detailed investigation of asphalt binder and asphalt mixture strength obtained with BBR is performed and presented. First, asphalt binder strength obtained with BBR is evaluated for different binder types and different cooling media: ethanol, potassium acetate and air. Statistical analysis is used to estimate the effect of these factors on the material response. Then, histogram strength testing is performed and the weakest link model and size effect theory is applied to compare BBR strength with the DTT results. Based on these results, a BBR strength test procedure for asphalt binders is proposed.

A general investigation on asphalt mixture size effect is performed next. Three-point bending tests, including mean strength test and histogram testing on different specimen sizes, are used to determine the statistical parameters characterizing the failure distribution of the Representative Volume Element (RVE) of asphalt mixture based on size effect theory. Results show that asphalt mixture has a typical quasibrittle behavior at low temperature. The relationship between Direct Tension and three-point bending is also investigated in this section.

Based on the results of the size effect investigation, asphalt mixture strength obtained with BBR is evaluated for the same three cooling media used for asphalt binder. Experimental results showed that the BBR beam is smaller than an effective material RVE and may be considered as part of the RVE substructure. Based on the BBR results, the brittle bundle model coupled with and approximation of the core of the RVE failure distribution are used to reconstruct the material RVE distribution. The RVE model is then verified by comparing the experimental results obtained on larger specimens with the prediction derived from the proposed model. Based on these results, a BBR strength test procedure for asphalt mixture is proposed.

At the end, a small experiment is performed to investigate the effect of cooling medium on asphalt mixture and asphalt binder creep compliance. From the statistical analysis, a clear difference is observed between the results obtained on binders tested in air and the results obtained on the same binders tested in ethanol and potassium acetate. No cooling medium effect is detected for asphalt mixture creep results.

CHAPTER 1

IDEA PRODUCT, CONCEPT, AND INNOVATION

Cracking due to low-temperature shrinkage stresses is the prevailing failure mode in asphalt pavements built in the northern part of the US and in Canada. This phenomenon is due to the contraction of the asphalt mixture under extreme temperature changes. Low temperature cracking manifests as a set of almost parallel surface-initiated transverse cracks of various lengths and widths. Due to water penetration, freeze and thaw cycles and traffic loads this can cause additional distresses dramatically affecting the service life of the pavement.

Therefore, good fracture properties are an essential requirement for asphalt pavements built in the cold regions. The current Superpave specifications address this issue through the use of strength and creep tests performed on asphalt mixture and asphalt binder specimens.

For asphalt binders two laboratory instruments were developed during the SHRP research effort to investigate the low temperature behavior of these materials: the Bending Beam Rheometer (BBR) (*AASHTO T 313-10-UL, 2010* (*1*)) and the Direct Tension Tester (DTT) (*AASHTO T 314-07-UL, 2007*(*2*)). These two devices are used to obtain the performance grade (PG) of asphalt binders in the US and Canada. The BBR is used to perform low-temperature creep tests on beams of asphalt binders conditioned at the desired temperature for 1 hour, while the DTT is used to perform low-temperature uniaxial tension tests at a constant strain rate and average stress and strain at failure are obtained.

Indirect Tensile test (IDT) or Brazilian tensile test was developed during SHRP program to obtain creep compliance and strength of asphalt mixtures (*AASHTO T 322-07-UL, 2007* (*3*). Unlike asphalt binder testing, mixture testing requires the use of expensive loading frames and expensive extensometers, which also require expensive and time consuming calibration and maintenance activities.

In a previous NCHRP Idea project (*4*), a simple test method to obtain the creep compliance of asphalt mixtures at low temperatures using the BBR device was developed. It becomes therefore important to develop a similar method to obtain the bending strength of asphalt mixture. This project investigates the idea of performing strength tests on asphalt binder and asphalt mixture beam specimens with the Bending Beam Rheometer (BBR) (Figure 1.1(a) and (b)). This would allow replacing the expensive IDT testing method with a simpler method that can be used to select asphalt materials with better cracking resistance and would provide the two key parameters used in the Mechanistic Empirical Pavement Design Guide (MEPDG) to predict low temperature performance. The use of the BBR three point bending

configuration can also be used to extrapolate the experimental strength results to larger specimens, which is not possible with the current IDT method because of the complicated size effect which is significantly affected by the loading boundary conditions (Figure 1.1(c)). In addition, using the BBR to obtain the bending strength of asphalt binders is also beneficial. The current DTT device is very expensive and there is limited service support provided for it.

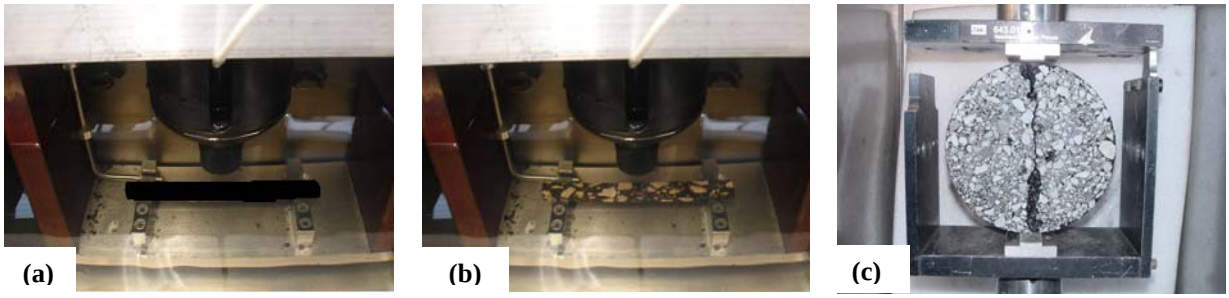

FIGURE 1.1 (a) BBR asphalt binder, (b) BBR asphalt mixture, and (c) IDT mixture tests

The next chapters detail the steps taken to develop the IDEA product. Chapter 2 briefly introduces size effect theory. Chapter 3 provides the results of the preliminary exploratory work on asphalt binder and mixture strength and the comparison with DTT and IDT respectively. Chapters 4, 5 and 6 present detailed investigations of strength for asphalt binder and asphalt mixture. Cooling medium influence on BBR results are evaluated. Size effect, representative volume element (RVE) modeling and difference between flexural and direct tension strength are included in these chapters. Chapter 7 presents a brief study on the effect of cooling medium on asphalt binder and asphalt mixture creep with the BBR. The conclusions and the plans for implementation are discussed in Chapter 8.

CHAPTER 2

REVIEW ON THE SIZE EFFECT OF STRUCTURAL STRENGTH THEORY

Size effect and scaling of materials properties were first discussed in the 1500s (*5*) but only after 1650s major advance were achieved (*6*). Nevertheless, significant progress in probabilistic and experimental investigation was obtained when extreme value statistics and weakest link model for a chain were formulated (*7*). The capstone of statistical size effect was laid by Weibull in 1939; he proposed for the tail of the extreme value distribution of the local strength of a small material element a power law with a threshold (*8*). Weibull theory applies to structures that fail at the initiation of a macrocrack with small fracture process zone (FPZ) and minimal stress redistribution (*9*). However, this is not true for quasibrittle materials such as Portland cement concrete and asphalt mixture for which the size of the inhomogeneities is not negligible compared to the structure size. In the recent past several research efforts were attempted to model the behavior of this class of materials based on linear elastic fracture mechanics (LEFM) (*10*), cohesive crack model (*11*) and fractal characteristics of cracks at different scales (*12*). More recently an energetic statistic approach to size effect of quasibrittle materials was successfully proposed by Bažant and co-workers (*13*, *14*, *15 16*).

This size effect formulation is used to analyze and evaluate the strength results obtained in this project. For this reason the next sections of this chapter provides an overview and a theoretical background on size effect theory for quasibrittle materials.

2.1 SIZE EFFECT TYPES

According to the deterministic theories of elasticity and plasticity, geometrically similar structures do not presents size effect, and their nominal strength, is defined as:

$$\sigma_N = \frac{cP_{\max}}{bD} \qquad [1]$$

where, σ_N is the nominal strength of the structure P_{max} is the maximum load at failure, D is the structure characteristic size (scaling dimension), b is the third dimension of the of the structure (b=constant), c is a constant such that σ_N represents the maximum principal stress of the entire structure. However, two main types of strength size effect can be identified for quasibrittle materials. Type I size effect, which is the only one considered in this research, occurs in notchless structures failing at macrocrack initiation from one representative volume element (RVE) of the material (*14*) (Figure 2.1(a)). Type II occurs in structures containing a large notch or a stress-free (fatigued) crack formed before reaching the peak load (*14*) (Figure 2.1(b)).

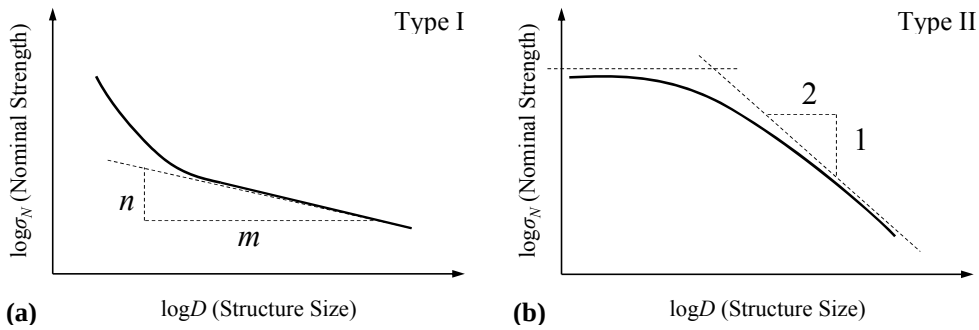

FIGURE 2.1 (a) Type I and (b) Type II size effect of structural strength

Type I size effect is typical of uniaxial and flexural failures, in which the RVE size is comparable with the thickness of the microcracking boundary zone where energy release and stress redistribution occur before the formation of a macrocrack. For structures in the small and medium size limit, the Type I size effect can be derived from the Taylor series expansion of the energy release function at zero crack length. At large size limit, the size effect is governed by the Weibull statistics.

Type I size effect can be alternatively derived from the weakest link model (WLM) (*14*). Due to the non-negligible dimension of the RVE the structure is statistically modeled as a finite chain of RVEs where the strength distribution of one RVE can be obtained from fracture mechanics of nano-cracks propagating by small, activation-energy controlled, random jumps through a nano-structure (*14* and *16*).

2.2 WEAKEST LINK MODEL

According to the weakest link model the structure can be represented as a chain of small material elements, known as Representative Volume Elements (RVE) (Figure 2.2).

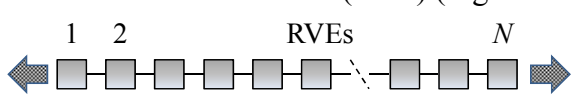

FIGURE 2.2 Weakest link model: chain of *N* RVEs

Each RVE, which is the smaller material volume that triggers the entire structure failure, represents an element of the structure model. Assuming the statistical independence of the random strength of

the RVEs and based on the joint probability theorem, the failure probability of the entire structure P_f made of N RVEs can be obtained as (*14*):

$$P_f(\sigma_N) = 1 - \prod_{i=1}^{N} \left[1 - P_1(s_i \sigma_N)\right] \qquad [2]$$

where P_1 is the cumulative distribution function (cdf) of strength of one RVE, σ_N is the nominal strength of the structure, s_i is the field of dimensionless maximum principal stress in the structure (fuction of the coordinate vector $\boldsymbol{x}$) such that $\sigma_N s_i$ corresponds to the maximum principal stress at the center of ith RVE. Based on experiments Weibull (*8*) realized that the left tail of the cdf of the material RVE follows a power law:

$$P_1 = \left[\sigma_N / s_0\right]^m \qquad [3]$$

where m is the Weibull moduls of the material (shape parameter) and s_0 is a material constant (scale parameter). Equation [2] can be rewritten in logarithm form and by approximating $\ln(1\text{-}x) \approx \text{-}x$ the following expression can be obtained (14, 16):

$$P_f(\sigma_N) = 1 - \exp\left\{-\sum_i^N \left(\frac{\sigma_N \langle s_i \rangle}{s_0}\right)^m\right\} = 1 - \exp\left\{-\int_V \left(\frac{\sigma_N \langle s(\boldsymbol{x}) \rangle}{s_0}\right)^m \frac{\mathrm{d}V(\boldsymbol{x})}{l_0^n}\right\} \qquad [4]$$

where l_0 is the dimension of the material RVE, $\langle s(\boldsymbol{x}) \rangle$ positive dimensionless stress field for the coordinates vector $\boldsymbol{x}(x,y)$ and $V(\boldsymbol{x})$ is the volume of the structure. Based on equation [4] the mean strength of the entire structure can be calculated as:

$$\bar{\sigma}_N = s_0 \Gamma\left(1 + \frac{1}{m}\right)\left(\frac{l_0}{D}\right)^{n/m} \left[\int_V \langle s(\boldsymbol{\xi}) \rangle^m \mathrm{d}V(\boldsymbol{\xi})\right]^{-1/m} \qquad [5]$$

where $\boldsymbol{\xi} = \boldsymbol{x}/D$ is the normalized coordinate vector, and $\Gamma(x)$ is the Eulerian gamma function. The coefficient of variation, ω_N (CoV), can then be derived from expression [5] as (*14*, *17*):

$$\omega_N = \sqrt{\frac{\Gamma(1+2/m)}{\Gamma^2(1+2/m)} - 1} \qquad [6]$$

2.3 BUNDLE MODEL

Another basic statistical model is the fiber bundle (or parallel coupling) (*14*) (Figure 2.3). The simplest and physically most meaningful approach to the load sharing after fiber break is to deduce load sharing from the physical fact that all the fibers are subjected to the same strain ε (*14*).

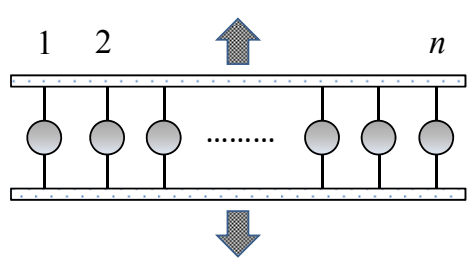

FIGURE 2.3 Bundle of fibers model

Fibers are numbered k = 1, 2...n in the order of increasing random values of strength σ_k. Fibers are also assumed to respond in elastic manner till the strength limit is reached, Same cross section A_f, same elastic modulus E_f and same strength cdf $F(\sigma)$ are assigned to each fiber. Two types of fiber behaviors can be identified after reaching the strength limit of the fiber: (a) brittle, when the stress

drops suddenly to zero, and (b) plastic, in which case the fiber plastically deforms at a constant stress σ^0 (*14*) (Figure 2.4).

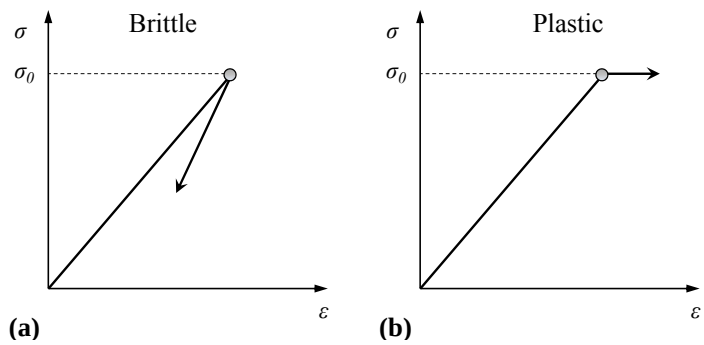

FIGURE 2.4 Behavior of (a) brittle fiber and (b) plastic fiber

For the purpose of this research only brittle fiber is considered since the related bundle model presents a simple formulation.

2.3.1 Brittle Bundle

The cumulative distribution function of strength σ of a bundle made on n brittle fibers can be derived from the following recursive formula (*14*, *18*):

$$G_n(\sigma) = \sum_{k=1}^{n} (-1)^{k+1} \binom{n}{k} F^k(\sigma) G_{n-k}\left(\frac{n\sigma}{n-k}\right) \qquad [7]$$

where $F^k(\sigma) = [F(\sigma)]^k$, $\sigma > 0$, $G_0 = 1$, $G_n(\sigma)$ is the strength cdf of the entire bundle with n fibers. When the strength cdf of each fiber has a power-law left tail with same exponent p then the cdf of strength of brittle bundle has also a power-law tail, and its exponent is np. In this case $F^k(\sigma) = \sigma^{kp}$ and expression [7] can be rewritten as (*14*):

$$G_n(\sigma) = \left[(-1)^{n+1} G_0 + \sum_{k=1}^{n-1} (-1)^{k+1} \binom{n}{k} \left(\frac{n\sigma}{(n-k)s_{n-k}} \right)^{(n-k)p} \right] \sigma^{np} = \left(\frac{\sigma}{s_n} \right)^{np} \qquad [8]$$

where s_{n-k} and s_n are scale parameters. It is clear that parallel couplings can raise the power-law tail exponent from 1 on
the nano-scale to any value, m, on the RVE scale (*14*).

2.4 RVE MODEL

Chain and bundle models can be used to reconstruct the mathematical model of material RVE. Based on recent studies (*14*, *15*, *16*) the failure probability of one RVE can be derived from atomistic fracture mechanics and a statistical multi-scale transition model where the failure probability of a nanoscale structure can be obtained by applying the transition rate theory to the discrete jump of a nano-crack. The transition from the nano-scale to the macro-scales of the RVE can be accomplished through a hierarchy of statistical chains and bundles (*14*, *15*, *16*). Figure 2.5 provides an example of hierarchical model of RVE structure.

Based on this framework, the strength distribution of one RVE can be approximated by a Weibull tail grafted on the left into a Gaussian cdf at a point with a probability between 10^{-4} and 10^{-3}. The grafted cdf of strength of one RVE can be expressed as (*14*, *15*, *16*):

$$P_1(\sigma) = 1 - \exp[-(\sigma / s_0)^m] \approx \langle \sigma / s_0 \rangle^m \qquad (\sigma_N \le \sigma_{gr})$$

[9a]

$$P_1(\sigma) = P_{gr} + \frac{r_f}{\delta_G \sqrt{2\pi}} \int_{\sigma_{gr}}^{\sigma_N} \exp\left\{ -\left[\frac{(\sigma' - \mu_G)^2}{2\delta_G^2} \right] \right\} d\sigma' \qquad (\sigma_N > \sigma_{gr})$$

[9b]

where σ is the maximum elastic principal stress at the center of the RVE, m is the Weibull modulus, s_0 is a scale parameter of the Weibull tail, $\langle x \rangle = \max(x, 0)$, μ_G and δ_G are the mean and the standard deviation of the Gaussian core alone. P_{gr} and σ_{gr} are the grafting probability and the grafting stress between the Gaussian and Weibull parts of the distribution respectively and r_f is a normalizing factor.

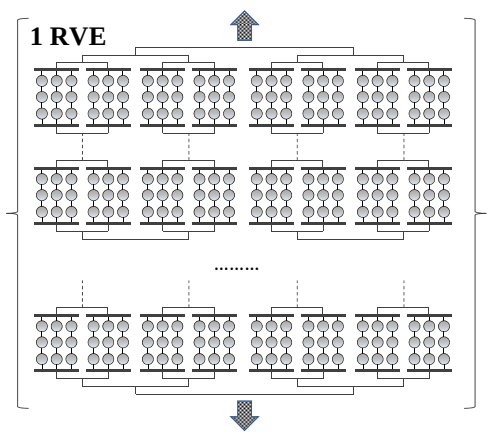

FIGURE 2.5 Example of RVE hierarchical model

The strength distribution of the entire structure can be calculated by mean of the joint probability theorem [2] and equations [9a] and [9b]. This results in a structure cdf that consists itself of two parts: below the grafting point the failure distribution still presents a Weibull cdf, while above the grafting stress, it follows a chain of Gaussian elements. For larger structure the Weibull tail penetrates into the Gaussian part eventually becoming completely dominant. Based on the failure cdf, the mean structural strength $\bar{\sigma}_N$ for structures of different sizes can be obtained as (*14*, *15*, *16*):

$$\bar{\sigma}_N = \int_0^1 \sigma_N \mathrm{d}P_f = \int_0^\infty [1 - P_f(\sigma_N)] \mathrm{d}\sigma_N$$

[10]

However, a closed form does not exist for equation [10] and a numerical solution is therefore needed to determine the effect of structure size, D, on mean strength for geometrically similar specimens. Based on asymptotic matching Bažant and co-workers (*13*, *14*, *15*, *16*) proposed an approximate expression for the size dependence of the mean strength:

$$\bar{\sigma}_N = \left[\frac{C_1}{D} + \left(\frac{C_2}{D} \right)^{rn/m} \right]^{1/r}$$

[11]

where m is the Weibull modulus, n is the number of dimensions to be scaled (n = 1, 2 and 3), and $C1$, $C2$, r are constants that can be determined using the following asymptotic conditions for small and

large-size of the mean strength size effect curve: $[\overline{\sigma}_N]_{D\to l_m}$, $[d\overline{\sigma}_N / dD]_{D\to l_m}$ and $[\overline{\sigma}_N / D^{n/m}]_{D\to\infty}$. l_m represents the smallest structure size used in the scaling. Equation [11] was found to fit very well Type I size effect curve (Figure 2.1a) for various types of quasibrittle materials (*13*, *14*, *15*, *16*). For this reason this expression is used throughout this research.

CHAPTER 3

EXPLORATORY EXPERIMENTAL WORK

This chapter present a summary of the experimental work conducted at the beginning of this investigation. The initial strength results obtained on asphalt mixture and asphalt binder with the new BBR device and the comparison with IDT (*3*) and DTT (*2*), respectively, are discussed.

3.1 BBR DEVICE

A new BBR device manufactured by Canon Instrument Company, called BBR-Pro, was used to perform testing (Figure 3.1). The new machine is equipped with a proportional valve that offers a much more complex control of the pressure in the air bearing system and is capable of providing, in load control mode, the loading pattern required by performing strength tests. The load cell capacity is 44N and the force range resolution is equivalent to 44/65,536=0.6713867mN/bit.

FIGURE 3.1 New BBR strength device

Windows based software is used to control the machine and assign commands through an external laptop/desktop computer. LDVT calibration is identical to the original BBR procedure and can be performed using the standard gauge blocks. To calibrate the load cells, up to nine 500 grams weights are used in conjunction with a thick steel beam. For each weight, the load deflection values are recorded and the software automatically performs compliance correction. Commands are assigned in steps with a maximum duration of 256 seconds in unit of ¼ of second (1s corresponds to 4 time units) starting from the initial selected load value and ending to the desired load.

3.1.1 Specimens Preparation

Asphalt binder beams are prepared according to AASHTO standard T313 (*1*). Asphalt mixture beams fabrication is detailed in the NCHRP 133 Final report (*4*) and it includes several cutting steps from the gyratory compacted (GC) cylinder specimens to the actual BBR beams. Figure 3.2 illustrates a scheme on how the beams are obtained from a cylindrical specimen. The dimension of the beam specimens are 125mm x 12.5 mm x 6.25mm and span 101.6mm.

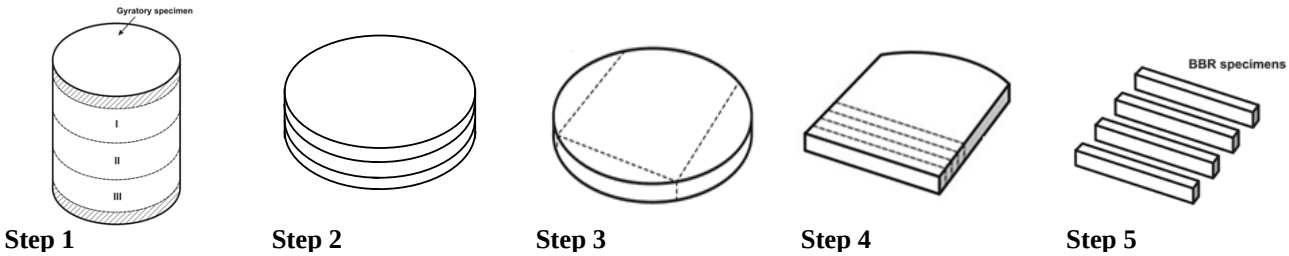

FIGURE 3.2 BBR asphalt mixture beams cutting procedure (*4*)

3.1.2 BBR Strength Calculation

The BBR nominal strength (maximum stress at peak load) σ_N and corresponding strain ε_N at the bottom of the thin beam (Figure 3.3) can be estimated from the dimensions of the beam, the applied load, and the measurement of deflection using equations [12] for asphalt binder and asphalt mixture.

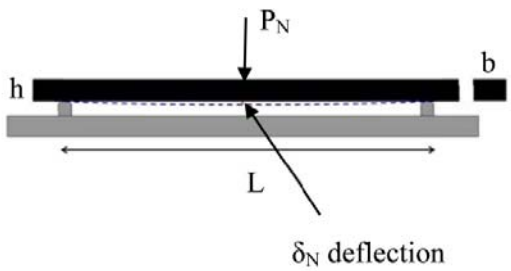

FIGURE 3.3 BBR strength test

$$\sigma_N = \frac{3P_N L}{2bh^2} \quad \text{and} \quad \varepsilon_N = \frac{6\delta_N h}{L^2}$$

[12]

where σ_N is the nominal strength (MPa), ε_N is the strain at failure, P_N is maximum measured load (N), L is the span length (mm), b is the width of the beam (mm), h is the thickness of the beam (mm) and δ_N is the deflection (mm) of the beam corresponding to the maximum load.

3.2 BBR ASPHALT MIXTURE STRENGTH

Two different asphalt mixtures are used for investigating BBR strength (Table 3.1). Mixture M6 was used to pave Cell6 during the second phase of MnROAD reconstruction during 2008 (*19*). It consists of 4.75mm Hot Mix Asphalt (HMA) made of a blend of two taconite aggregates and manufactured sand. Mixture M84 was used for the farm equipment study performed at MnROAD (*20*) and has a maximum aggregate size of 19.0mm.

TABLE 3.1 Asphalt mixtures

ID	Type	Binder PG	Aggregate	Target Air Voids (%)
M6	Cell 6 MnROAD	PG 64-34	Taconite	7
M84	Cel 84 MnROAD	PG 58-34	Various	7

Asphalt mixture loading procedure is implemented based on previous research results (*21*) in which two different loading rates were applied. In this investigation, two similar loading rates are selected: 16.64N/min and 16.64/4 = 4.16N/min based on the capabilities of the new BBR and with the purpose of evaluating loading rate effect; two different temperatures (low PG+10ºC and low PG+22ºC) are also considered for testing. Asphalt mixture tests are performed in an ethanol bath as in the current standard for asphalt binder creep tests (*1*). Twenty four beam replicates for each of the four factor level combinations (treatments T1 to T4) given by loading rate and temperature are used. Table 3.2 presents the results obtained (CoV stands for coefficient of variation).

TABLE 3.2 Asphalt mixtures BBR strength results

ID	Mix Cell	Binder PG	Rate N/min	Temp °C	Mean Strength MPa	CoV %	Mean Strain -	CoV %
M6-T1	6	64-34	4.16	-24	9.8	6.6	0.0019	13.8
M6-T2	6	64-34	16.64	-24	10.4	9.2	0.0015	10.6
M6-T3	6	64-34	4.16	-12	8.1	6.6	0.0081	11.5
M6-T4	6	64-34	16.64	-12	9.3	8.1	0.0058	13.4
M84-T1	84	58-34	4.16	-24	6.4	11.9	0.0008	14.7
M84-T2	84	58-34	16.64	-24	6.5	11.2	0.0007	18.0
M84-T3	84	58-34	4.16	-12	6.3	12.0	0.0030	22.6
M84-T4	84	58-34	16.64	-12	6.8	12.5	0.0020	20.6

Numerical results shows a clear difference in strength between mixture M6 (higher mean strength) and M84, suggesting that BBR strength test is capable of distinguishing among different materials. The effect of the different treatments (loading rate and temperature) on stress and strain is clearly evident (Figure 3.4); CoV stands for coefficient of variation.

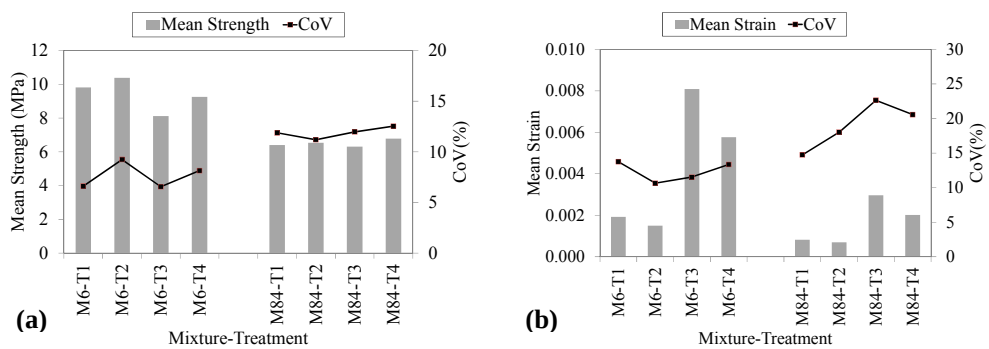

FIGURE 3.4 (a) Strength and (b) strain bar charts for asphalt mixture BBR testing

The statistical distribution of asphalt mixture strength is qualitatively evaluated from the stress strain curve and by means of strength histograms (see Chapter 2) in the Weibull plane (*8*, *22*); Figures 3.5a and 3.5b present an example stress strain curve and strength histogram for mixture M6 at T=-24°C and for a loading rate=4.16 N/min.

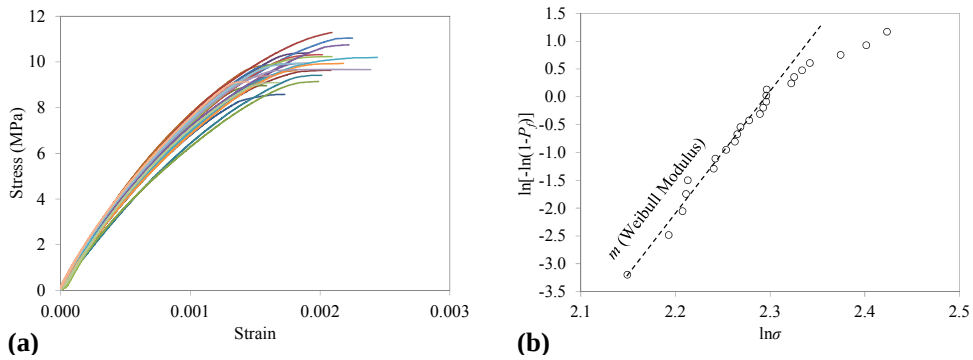

FIGURE 3.5 (a) Stress strain curves and (b) strength histogram for mixture M6 T=-24°C, rate=4.16 N/min

The curves of the different replicates are fairly close and consistent for the specific temperature and loading rate conditions. Strength Histogram suggests that there may be a left Weibull tail in the failure distribution of asphalt mixture strength obtained with BBR.

Asphalt mixture air voids of BBR beams were evaluated so that they could be included in the statistical analysis that is next performed. Air void measurement of individual thin mixture beams are obtained using Digital Image Processing (DIP). The DIP procedure implemented in MATLAB (*23*) consisted in a series of steps by which the RGB color image (720dpi) is transformed into a black and white image where the mixture air voids are detected through global thresholding (*23*) over the entire cylindrical gyratory compacted specimen. Figure 3.6 provides an example of air voids detection for a BBR beam of mixture M84.

FIGURE 3.6 (a) Original RGB and (b) air voids (white pixels) images for asphalt mixture M84 BBR beam

The nominal strength and failure strain obtained from BBR tests is evaluated using Analysis of Variance (ANOVA) to determine which factors affect the response (strength and strain). Temperature and loading rate are set as factors; each of the factors had two levels. Mixture type is used as a block (*24*) since different responses are expected for the two mixtures. Air voids of each beam are used as covariate (*24*) and the effect on the response evaluated. Tables 3.3 and 3.4 presents the coefficients estimates obtained from ANOVA.

TABLE 3.3 Coefficients estimate for asphalt mixture BBR strength from ANOVA

Coefficients	**Estimate**	***t***	***p*-value**
Intercept	12.229	14.0	10E-8
Voids	-.400	-2.6	**0.011**
Mixture M84	-3.151	-19.7	**10E-8**
Temperature=-12°C	-.662	-5.4	**10E-8**
Rate=4.16N/min	-.564	-4.6	**10E-8**

TABLE 3.4 Coefficients estimate for asphalt mixture BBR strain from ANOVA

Coefficients	Estimate	*t*	*p*-value
Intercept	-6.442	-248.3	10E-8
Mixture M84	-.910	-39.0	**10E-8**
Temperature=-12°C	1.212	36.8	**10E-8**
Rate=4.16N/min	.210	6.4	**10E-8**
[Temperature=-12°C] * [Rate=4.16N/min]	.163	3.5	**0.001**

In case of strength voids covariate is highly significant at a 0.05 significance level and at an increase in voids correspond a decrease in strength. A clear difference in mixture type is detectable with mixture M84 having lower mean strength value compared to mixture M6. Temperature and loading rate significantly affect strength results with lower strength values for higher temperature (T=-12°C) and lower loading rate (4.16N/min). In case of strain a simple linear model suggests that all the factors are statistically significant except air voids. Mixture M84 provides a lower strain results compared to mixture M6 while higher temperature, lower loading rate and their interaction increase the values of the response. Due to the significant effects of voids it is therefore important to avoid testing BBR beams specimens obtained from the parts of the mixture slice (Figure 3.2) too close to the wall of the GC sample.

3.3 COMPARISON OF BBR AND IDT ASPHALT MIXTURE STRENGTH

The same two asphalt mixtures of Table 3.1 are used to for IDT strength tests (*3*). Tensile strength is estimated as:

$$\sigma_{IDT} = \frac{2P_N}{\pi b D} \qquad [13]$$

where σ_{IDT} is the tensile strength (MPa), P_N is the failure load, representing the load at which the difference between vertical and horizontal deformation is maximum, b is specimen thickness (mm) and D is specimen diameter (mm).

To avoid damage to the LVDT's, P_N is usually assumed as the peak load; for this reason a correction formula proposed in a past research (*25*) can be used to evaluate the tensile nominal strength σ_{IDT}^{U} obtained with this method:

$$\sigma_{IDT}^{U} = (0.78\sigma_{IDT}) + 38 \qquad [14]$$

where σ_{IDT}^{U} and σ_{IDT} are expressed in psi.

IDT strength test are performed on twenty-one and twenty replicates for mixture M6 and M84 respectively at a single temperature of T=-24°C (low PG+10°C). IDT results are compared with the analogous BBR tests performed at the same temperature and higher loading rate of 16.64 N/min. Table 3.5 and Figure 3.7 present the mean strength values for BBR, IDT and corrected IDT [14]; CoV stands of coefficient of variation.

TABLE 3.5 Asphalt mixtures BBR and IDT strength

Mix	BBR		IDT		IDT Correction	
ID	Mean Strength	CoV	Mean Strength	CoV	Mean Strength	CoV
M6	10.4	9.2	6.0	5.1	4.9	5.1
M84	6.5	11.2	3.7	7.8	3.2	7.8

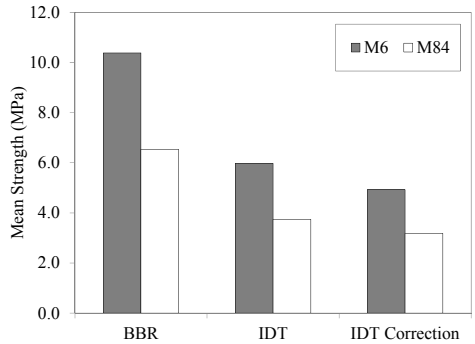

FIGURE 3.7 BBR and IDT mean strength

Analysis of Variance (*24*) is used to analyze asphalt mixture strength data by setting mixture type (M84 and M6 – control) and test type (IDT and BBR - control) as factors. Two separate statistical analyses were performed in which BBR strength is first compared to IDT values and then to IDT corrected values. Tables 3.6(a) and 3.6(b) show the statistical output.

TABLE 3.6 ANOVA parameters estimation: (a) BBR vs IDT strength and (b) BBR vs corrected IDT strength

Coefficients	**Estimate**	***t***	***p*-value**
Intercept	2.337	148.1	10E-8
Mixture M84	-0.467	-25.0	**10E-8**
Test IDT	-0.551	-29.4	**10E-8**

(a)

Coefficients	**Estimate**	***t***	***p*-value**
Intercept	2.330	150.0	10E-8
Mixture M84	-0.452	-24.6	**10E-8**
Test IDT corrected	-0.730	-39.6	**10E-8**

(b)

Both analyses show that BBR strength values are significantly higher compared to IDT measurements at a statistical significance level of 0.05. As expected, mixture M6 presents higher strength than mixture 84, while no interaction effects are detected between test type and mixture.

No further analysis is performed on IDT strength data. This is because different past research efforts showed that Indirect Tensile, Brazilian and Split strength tests are dominated by a non-unique and irregular size effect (*26*, *27*, *28*, *29*, *30*, *31*) that may significantly limit the possibility of extrapolating the experimental results to larger structures. The complexity of the observed behavior can be explained with the rate dependence of the splitting strength tests and especially with the high sensitivity of this type of test to the boundary conditions (*17*). Rocco (*32*) showed that the presence and the height of second stress peak in a stress-diametral-extension curve are highly dependent on the loading strip to specimen diameter ratio h/D. To improve the test validity it was recommended an h/D such that the maximum stress corresponds to the first peak; however this approach still presents a significant limitation since the testing apparatus geometry depends on the specimen dimensions. Two analytical size effect formulations were proposed by Bazant and co-workers (31) to predict the IDT strength for different specimen sizes. However, the sharp rise in strength for larger specimen sizes is not confirmed by other experimental data, therefore limiting the possibility of using this type of size effect approach. An example of mean strength dependence on the structure size for IDT is shown in Figure 3.8.

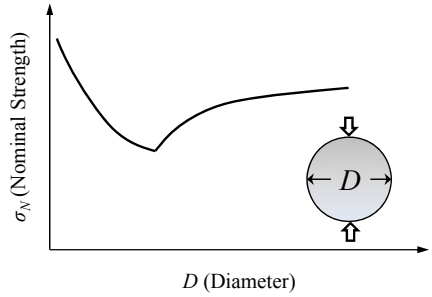

FIGURE 3.8 IDT mean strength size effect curve

This brief analysis shows that strength data obtained from Indirect Tensile tests are difficult to interpret and extrapolation of results to larger structures can become prohibitive. This suggests that a different and simpler type of testing configuration such as three point bending should be used to obtain strength values.

3.4 BBR-DTT ASPHALT BINDER STRENGTH COMPARISON

Three asphalt binders used in a different research effort (*33*), for which DTT results in potassium acetate (PA) were available, are selected for this study: PG 58-28 (unmodified), PG 58-34 (SBS modified) and PG 64-22 (unmodified). The first two asphalt binders are short and then long termed aged prior to testing; bending strength tests are performed using the new BBR device (Figure 3.1) in ethanol for both aging conditions. Short term aging is performed according to Rolling Thin-Film Oven Test procedure (RTFOT) (*34*) and long term aging is performed according to Pressurized Aging Vessel (PAV) method (*35*). DTT strength results were available for both aging conditions at which BBR strength tests are run.

Binder PG 64-22 is used in the second part of the experimental phase, in which BBR strength tests are run in ethanol and in potassium acetate. All tests results for this asphalt binder are obtained for RTFOT condition. To further investigate the effect of cooling medium, additional testing in potassium acetate is performed on PG 64-22 binder and also on PG 58-28.

Asphalt binder nominal strength obtained with BBR is calculated according to equation [12], while asphalt binder DTT (Figure 3.9) nominal strength (and strain at failure) is obtained from equation [15]:

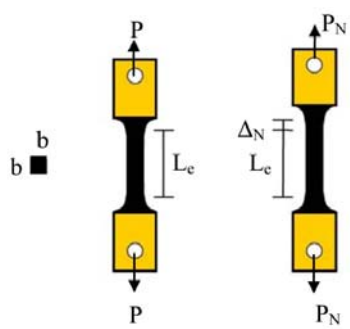

FIGURE 3.9 DTT strength test

$$\sigma_N = \frac{P_N}{A} \quad \text{and} \quad \varepsilon_N = \frac{\delta_N}{L_e} \qquad [15]$$

where σ_N is the stress at failure (MPa), ε_N is the failure strain, P_N is failure load (N), L is the span length (mm), $A=b\text{x}b$ is the original area of the cross section (mm^2), δ_N is the elongation at failure (mm) and L_e is the effective gage length (33.8mm).

The loading procedure for the first two asphalt binder is set in such a way that DTT and BBR times to failure for PAV aged binder tested at lower PG+10ºC are similar. This approach is selected based on the fact that the cohesive law, governing the fracture process zone (FPZ) propagation, is rate dependent and consequently time dependent. By selecting similar times to failure for the two tests, the FPZ propagation is imposed to occur with the same rate (*36*). This approach is taken for obtaining a procedure that facilitates the comparison of DTT and BBR strength since the two tests are performed using different loading procedures: displacement and load control, respectively.

A loading rate of 5.60N/min is used during BBR testing to match the time to failure in DTT. A second loading rate equal to 5.60/4 = 1.40N/min is also considered to investigate the effect of loading rate on the measured strength obtained with BBR. Two different tests temperature are used: low PG+10ºC and PG+4ºC. The next two figures show the strength results for binder PG 58-34 (Figure 3.10 and 3.11); CoV stands of coefficient of variation.

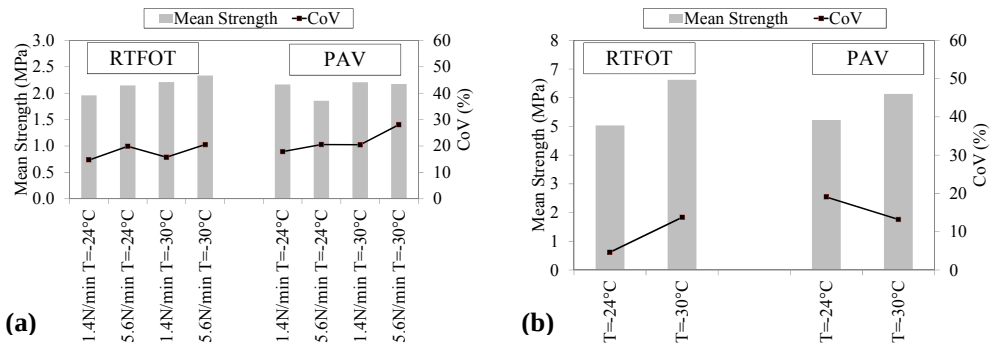

FIGURE 3.10 (a) BBR and (b) DTT strength bar charts for asphalt binder PG58-34

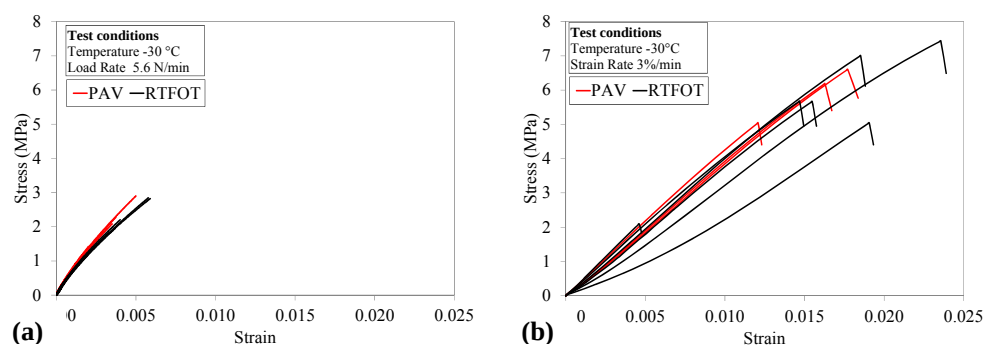

FIGURE 3.11 (a) BBR and (b) DTT stress strain curves for asphalt binder PG58-34 T=-30 ºC

Visual comparison indicates that DTT curves (Figures 3.11) are spread out with no clear distinction between RTFOT and PAV aging conditions. BBR stress strain curves present a smaller variation; a better separation of the two aging conditions is observed for both binders suggesting a better repeatability. BBR strength is much smaller than DTT results.

ANOVA analysis was also performed to evaluate effect of binder type, temperature, aging and tests type on strength results. Table 3.7 presents the results of the analysis.

TABLE 3.7 Coefficients estimates for DTT vs. BBR asphalt binder strength from ANOVA

Coefficients	**Estimate**	***t***	***p*-value**
Intercept	4.862	33.6	10E-8
Binder=PG 58-28	-0.529	-5.3	**10E-8**
Temperature=Low PG+4	1.024	5.0	**10E-8**
Test=BBR	-2.694	-17.2	**10E-8**

[Test=BBR] * [Temperature=Low PG+4°C]	-0.965	-4.1	**10E-8**

Binder, temperature, test type and interaction between test and temperature are all significant terms. Binder PG 58-28 gives lower strength values compared to PG 58-34. No aging effect on the response is found. Lower testing temperature results in higher strength. Measurements obtained from BBR tests are much lower than those generated from DTT.

3.4.1 Size Effect Comparison

Strength results obtained on asphalt binder PG58-34 and PG58-28 clearly show that there is a significant difference between the values measured with BBR and DTT. However, the two tests are performed under different types of loading, three-point bending and direct tension, and the volumes of the specimens are significantly different: 9921.9mm^3 and 1945.9mm^3 for BBR and DTT, respectively. The dependence of structural strength on the structure size and geometry can be explained using the well-established size effect theory (see Chapter 2).

BBR and DTT specimens share the same failure mechanism, where the peak load is reached once a macro-crack initiates from one representative volume element (RVE). Therefore, the structure can be statistically represented by a chain of RVEs. In the present study, the grain size of the binder is on the nanoscale. Therefore, it may be assumed as an approximation that the RVE size is almost negligible compared to the specimen size. Based on equations [4] and [5] and by using the elastic stress field it is possible to predict the strength of DTT specimens from the strength of BBR specimens. For this purpose a Weibull modulus m=10 was chosen based on the preliminary tests on strength histogram. Table 3.8 shows the comparison between predicted and measured DTT strengths for binder PG 58-28 and PG58-34.

TABLE 3.8 Coefficients estimates for DTT vs. BBR asphalt binder strength from ANOVA

Binder	**Aging**	**T (ºC)**	**Measured Mean Strength (MPa) BBR**	**DTT**	**Ratio (%)**	**Corrected Mean Strength (MPa) BBR to DTT**	**Ratio (%)**
PG58-28	PAV	-18	2.1	4.2	51.3	1.4	32.6
PG58-34	PAV	-24	1.9	5.2	35.5	1.2	22.5

The predicted DTT strength is three to four times lower than the measured one and other factor(s) are responsible for the significant difference. The other significant difference between DTT and BBR tests is the cooling medium: DTT specimens are cooled using potassium acetate and BBR specimens are cooled using ethanol. Based on previous research (*37*), which showed significant difference for DTT strength in potassium acetate (PA) and ethanol (E), a new set of experiments is performed on PG64-22 binder in RTFOT condition. BBR strength tests are run in ethanol and then in potassium acetate at PG - 2ºC to evaluate the effect of cooling medium on strength measurements. From the nominal stress strain curves in Figure 3.12, it is evident that BBR mean strength in potassium acetate is almost 4.5 times higher than BBR mean strength in ethanol.

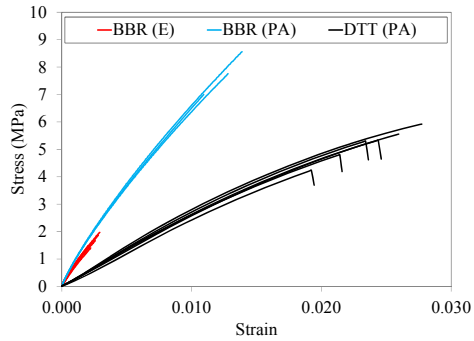

FIGURE 3.12 Cooling medium effect on BBR stress strain curves for binder PG64-22

Using the same Weibull approach it is possible to estimate the corrected strength for the new test results. As explained at the beginning of section 4, BBR loading rates are selected such that BBR time to failure is comparable with the time to failure of DTT. Due to the significant difference in strength, different loading rates are used for BBR tests in ethanol and potassium acetate, respectively. Table 3.9 summarizes the test results as well as the corrected values for the BBR strength in ethanol (E) and in potassium acetate (PA).

TABLE 3.9 BBR and DTT results and comparison for different cooling media

Test	**Rep.**	**Cooling Medium**	**Loading Rate**	**Mean Strength**	**Corrected BBR Mean Strength**	**Ratio Corrected BBR mean strength DTT mean strength**
Type	**#**		**N/min**	**(MPa)**	**(MPa)**	**%**
BBR-E	5	E	7.2	1.7	1.0	18.4
BBR-PA	3	PA	24	7.8	4.8	**85.1**
DTT	4	PA	-	5.7	-	

The corrected BBR strength in ethanol is almost five times smaller than DTT strength, while the corrected BBR strength in potassium acetate is fairly similar to DTT strength, since the 15% difference is less than testing variability. The effect of cooling medium on BBR strength is further evaluated for binders PG58-28 and PG64-22, using the same loading rate (7.2N/min), not dependent on DTT time to failure, and same testing temperature (T = -24°C) . The results of these tests provide further evidence of the strong effect of ethanol on the flexural strength, with a very similar impact on both asphalt binders (21-22% strength ratio BBR/DTT).

Based on the limited literature review, it can be hypothesized that both chemical interaction (with ethanol) and diffusion occurred in the asphalt binders specimens conditioned and tested in ethanol. This effect is known in literature as Environmental Stress Cracking (ESC) (*38*, *39*, *40*).

3.5 CONCLUSIONS

A number of conclusions can be drawn from the exploratory experimental work. For asphalt mixtures, BBR strength tests can be performed. Parameters such as air voids, temperature and loading rate influence the response. The statistical failure distribution presents a Weibull tail and thus size effect need to be further investigate. The IDT has limitations as a strength test due to its complex size dependence of the response; this is not the case for bending strength test.

For asphalt binders, BBR strength is mainly influenced by temperature while the aging condition is not statistically significant. Based on the comparison of BBR and DDT results a strong dependence on the cooling medium is also found.

Based on these findings, a more detailed investigation on the cooling medium effect on material strength and the RVE properties of both asphalt binder and asphalt mixture is performed next.

CHAPTER 4

BBR ASPHALT BINDER STRENGTH

In this chapter asphalt binder strength obtained with the BBR is further investigated. Cooling medium, aging and conditioning time are considered in the analysis, and based on size effect approach, BBR and DTT are compared.

4.1 MATERIALS AND TESTING

Two asphalt binders are used: a plain binder Citgo PG 58-28 and a modified Elvaloy binder MIF PG58-34. A single testing temperature is set as low PG+4°C. This is done to extend the range of temperatures studied with respect to the work performed in Chapter 3. Time to failure of BBR strength tests is selected based on the values of the corresponding DTT (*2*) tests for the same two binders performed at the same temperatures. This limits the rate dependence of the fracture process zone (FPZ). Given the condition selected this is in the range of 15-20s. Aging (RTFOT (*34*) and PAV (*35*)), conditioning time (1h and 20h) and cooling medium are considered in the analysis. Binder type is used as block since differences are expected between Citgo and MIF binders. Three type of cooling medium are considered: ethanol (E), potassium acetate (PA) and air (A). Table 4.1 presents the experimental design for BBR strength tests. BBR nominal strength is calculated according to equation [12] and the mean obtained over five replicates per each testing condition.

TABLE 4.1 Variables Definition for Statistical Analysis

Independent Variable	Type / Description
Binder Type	1 – Citgo; 2 – MIF (Control)
Aging	1 – RTFOT; 2 – PAV (Control)
Cooling Medium	1 – PA; 2 – A; 3 – E (Control)
Conditioning Time	1 – 20h; 2 – 1h (Control)

In the second experimental part, BBR strength histogram testing is performed on a larger number of replicates, 20 and 21 for Citgo and MIF, respectively. Results are compared to DTT mean strength through size effect theory based on the weakest link model. Only PAV aging (*35*) and 1h conditioning time are considered for this phase of the investigation.

4.2 MEAN NOMINAL STRENGTH RESULTS

Figure 4.1a and 4.1b shows the mean strength obtained from BBR testing for all the condition outlined in Table 4.1; CoV stands for coefficient of variation (%). Figure 4.2a and 4.2b presents an example of stress strain curve.

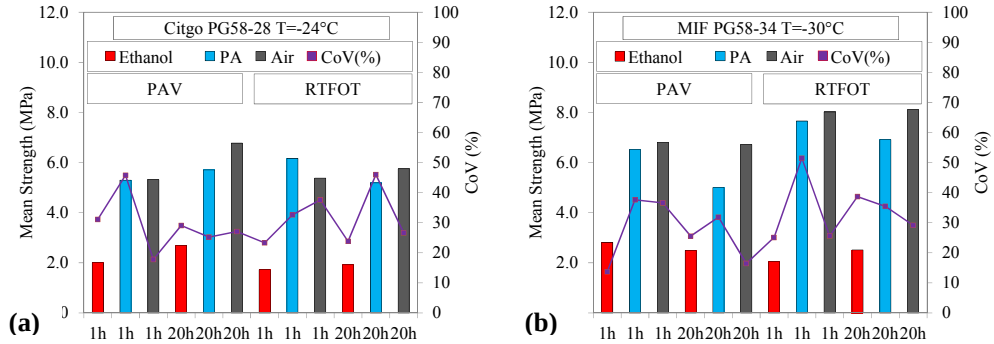

FIGURE 4.1 BBR mean strength for asphalt binder (a) Citgo PG58-25 and (b) MIF PG58-34

Stress strain curves shows that there is an increase in asphalt binder strength moving from the tests performed in ethanol, to potassium acetate and air, with a slightly larger dispersion for the results in potassium acetate. It can be visually observed that much larger strength values are obtained in PA and air compared to ethanol, and similar measurements are found for PA and air.

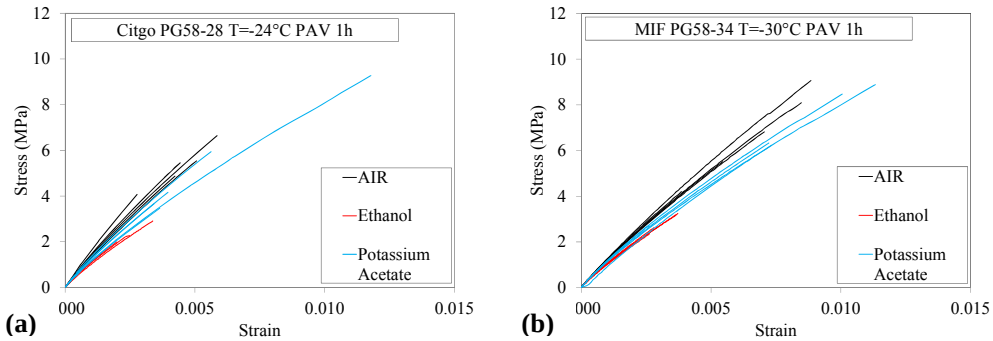

FIGURE 4.2 BBR stress-strain curve for asphalt binder (a) Citgo PG58-25 and (b) MIF PG58-34

4.2.1 Statistical Analysis

In Chapter 3, it was found that BBR strength presents a failure distribution (statistically a cumulative distribution function – cdf) with a Weibull tail. To better take into account this finding, a non-parametric statistical analysis (*41*, *42*) based on ANOVA (*24*) is performed to evaluate the significance of the different factors assumed in the experimental design (Table 4.1). Table 4.2 summarizes the output of the statistical analysis.

TABLE 4.2 Statistical analysis of BBR asphalt binder strength

Factor	Coefficients	Estimate	*t*	*p*-value
Binder Type	Citgo	-1.222	-10.9	**10E-08**
	MIF	-0.832	-7.4	**10E-08**
Cooling Medium	Potassium Acetate	1.450	10.6	**10E-08**
	Air	1.631	11.9	**10E-08**
	Ethanol	Control	-	-

Non parametric statistics shows that factors such as aging and conditioning time are not statistically significant, confirming the findings of Chapter 3. No intercept is needed by the statistical model. As expected the response is binder dependent, and obviously strongly affected by the cooling medium, with much higher values for potassium acetate and air. Furthermore, the Tukey–Kramer method (*24*), which is a single-step multiple comparison, shows there is no difference in mean

strength between specimens tested in potassium acetate and air. Based on these results in the next section asphalt binder BBR strength in air is compared to DTT strength in potassium acetate.

4.3 BBR – DTT STRENGTH COMPARISON

The strength results obtained from BBR histogram tests in air for binder Citgo and MIF (section 4.1) are first plotted in the Weibull plane (Figure 4.3a and 4.3b) where P_f represent the failure probability (cdf) of the BBR specimen. Citgo binder presents a very different behavior compared to MIF. The first one follows an almost straight line in the Weibull plane meaning its cdf is mainly governed by the Weiubull statistics, while MIF binder presents a clear quasibrittle behavior with a Weibull tail. Similar Weibull moduls, *m*, where found: 9 and 10 for Citgo and MIF, respectively.

For this reason and to compare the strength results with the DTT strength two different analyses are used. In the case of the plain asphalt binder Citgo the size of the RVE is assumed as negligible since at the nanoscale level. A simple Weibull statistics approach based on the Weakest Link model [2] and on equations [4] and [5] is applied to fit the experimental results (Figure4.3a solid black line).

For modified asphalt binder MIF, the dimensions of RVE cannot be neglected due to its quasibrittle strength distribution. Based on literature review on modified asphalt binders (*43*) and on size effect theory for quasibrittle materials (*14*, *15*, *16*), a 2D-scaling RVE with a characteristics size l_0=50μm is assumed and the BBR beam of asphalt is schematized as an assembly of RVEs. Weakest link model (equation [2]) is used to fit the experimental results based on the grafted CDF model of the material RVE (equations [9a] and [9b]). The model fitting is shown in Figure 4.3b.

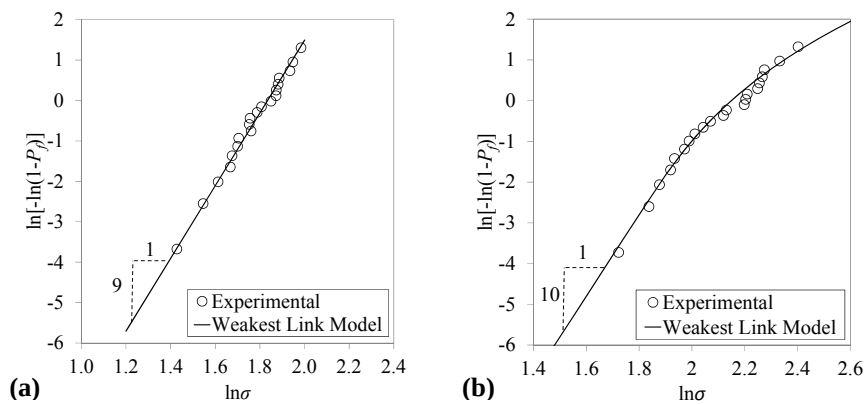

FIGURE 4.3 BBR strength histograms and WLM for asphalt binder (a) Citgo PG58-25 and (b) MIF PG58-34

Based on statistical parameters obtained during model fitting, BBR strength of both asphalt binder is converted into the corresponding DTT strength and compared with experimental DTT results for the same binders tested in potassium acetate. Eight replicates are used to determine DTT mean strength. Table 4.3 presents the results of the comparison.

TABLE 4.3 Comparison between BBR and DTT asphalt binder strength

Binder Type	PG	BBR Strength (MPa)	BBR to DTT Strength (MPa)	DTT Strength (MPa)	(BBR to DDT)/DTT %
Citgo	58-28	5.8	3.7	3.9	**94.3**
MIF	58-34	8.3	5.4	5.8	**94.0**

A minimal difference (about 6%) is observed between the converted BBR strength and the experimental DTT data for both asphalt binders; this is less than the experimental error (20%). For modified binder MIF a simpler Weibull solution, used for plain binder Citgo, cannot be used, since it would lead to a severe under prediction of the DTT mean strength, with a difference of more than 30%.

4.4 CONCLUSIONS

Several conclusions can be drawn from the results presented in this chapter. Asphalt binder BBR mean strength obtained in ethanol is much lower than those in measured in potassium acetate and air; the last two are comparable and statistically similar. This confirms the cooling medium effect on binder strength.

BBR strength histograms shows a binder dependence of the material failure distribution and thus of the RVE cdf itself. Plain binder shows a typical Weibull statistics pattern with a strong brittle behavior, while modified binder presents a quasibrittle pattern. This can most likely be attributed to the polymer modification and consequently to the non-negligible dimension of the material RVE which still remain very small.

Weakest link model can be used to transform the BBR flexural response into a DTT uniaxial stress; conversion shows that BBR strength obtained in air and DTT strength obtained in potassium acetate results are very similar. These findings suggest that air is a suitable cooling medium to perform BBR strength tests on asphalt binder.

4.4.1 BBR Test Procedure for Asphalt Binder Strength

The following steps briefly summarize the BBR strength test procedure:

- Prepare BBR beam specimens according to AASTHO T313-10-UL (*1*): for histogram testing prepare 24 replicates, for mean strength prepare 6 replicates;
- Condition specimens for 1h in air at the desired testing temperature (low PG+4°C or low PG+10°C);
- Select loading rate to fail specimens within 15-20s (this reduces viscoelastic effects) and perform tests;
- Compute nominal strength according to equation [12];
- Compute mean (average) strength (for mean strength tests);
- Plot histogram (for histogram strength tests) and by using the weakest link model determine the RVE parameters; convert BBR strength to direct tension strength through weakest link model.

CHAPTER 5

ASPHALT MIXTURE STRENGTH SIZE EFFECT

This chapter presents a general study on the size effect of asphalt mixture strength at low temperature. The first objective is to verify if asphalt mixture presents a size effect of Type I (*13*, *14*, *15*, *16*) (see Chapter 4.1). The second objective is to provide an initial estimate of asphalt mixture RVE dimensions and statistical properties. By knowing these two aspects it is then possible to better analyze the strength measurement obtained from small BBR mixture beams (Chapter 6).

To achieve such objectives a method to indirectly determine the strength distribution function (cdf) of the material RVE is used. The method is derived within the framework of the finite weakest link model (WLM, equation [1]). By inverting this model the cumulative distribution function of structural strength (equations [9a] and [9b]) is directly determined from the parameters of the mean size effect curve (equation [11]) (*13*, *14*, *15*, *16*). A set of experiments on asphalt mixture at a low temperature, including both strength histograms and the mean size effect of asphalt mixture specimens of different sizes is used to perform this investigation.

5.1 MATERIALS AND TESTING

The experimental phase of this investigation is limited to a single asphalt mixture prepared with an asphalt binder (7.4% by weight) from performance grade PG 64-34 and with a blend of aggregates consisting of taconite aggregates (55% of MIN TAC tailings and 10% of ISPAT tailings) and pit sand (35%). The nominal maximum aggregate size is 4.75mm and the nominal average aggregate size is 1.22mm. Since the RVE size for quasibrittle materials (*14*, *21*) is about two times of the size of material inhomogeneities (*14*), the volume of one RVE V_0 for this particular asphalt mixture is about 14.4 mm^3.

Since a mean size effect curve such that in Figure 2.1a is expected to be obtained from testing a sufficient a large size range is required. In this study, the size effect tests are carried out by using three-point bend beams strength tests in air at low temperature. However, the sizes of the testing machine and the climate chamber impose a limit on the beam size. To overcome such a difficulty, the change in failure probability in a structure with different geometry and stress field can be exploited. Therefore, in order to reach a large size range for the present study, an additional set of mean strength test on direct tension specimens is prepared. The size of the specimen is selected to be much larger than the size of the RVE. This guarantees that the strength cdf of the direct tension specimen follows the Weibull statistics which provides a simple conversion method to the equivalent size of the three-point bend beam.

Tests specimens are obtained from twenty-six slabs of asphalt mixture (size 380 mm by 200 mm) compacted at target air voids of 7% by mean of a Linear Kneading Compactor (LKC). In order to optimize asphalt mixture preparation and specimens cutting two different slab thicknesses were used: 50 mm and 75 mm. Since 2D scaling was considered in this study, asphalt mixture beams of similar geometry with constant width *b*=40mm, depth to span ratio equal to 1:6 and size ratio $1:\sqrt{3}:3$ were prepared for three point bending tests (Figure 5.1).

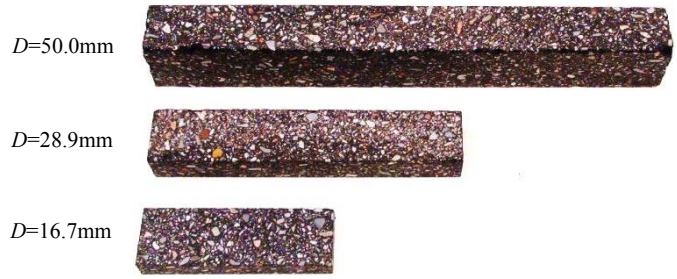

FIGURE 5.1 Asphalt mixture beams

A forth specimen type was prepared for DT tests by cutting one-size asphalt mixture prisms. The thickness of the beams, *D*, and the width of the prism are selected as characteristic dimensions for the three-point bending and direct tension specimens, respectively (Figure 5.2a and 5.2b). A temperature T=-24°C, corresponding to the low limit of binder PG+10°C and close to the glass transition was set for testing. Both three-point bending and DT tests are conducted in load-control mode; this is because only the peak load is of interest for this study. In order to minimize the loading rate effect and impose a constant loading rate of the fracture process zone a time to failure of about 5 minutes is set for all the specimen sizes (*17*, *36*). Therefore, different loading rates are used for different specimen sizes and geometries.

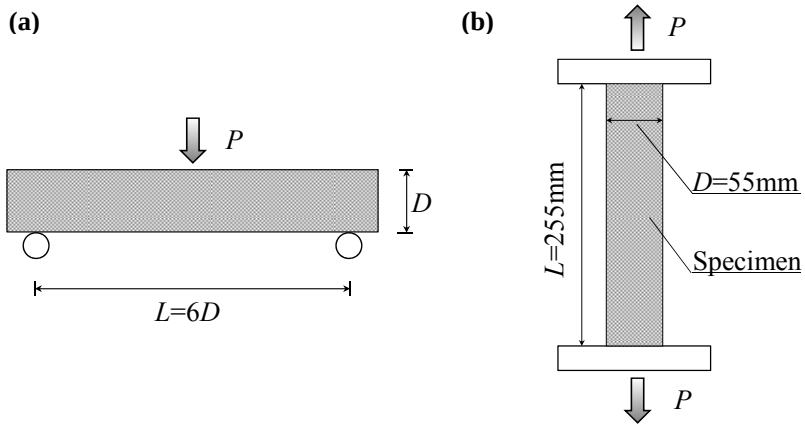

FIGURE 5.2 (a) Three point bending and (b) Direct tension tests

Nominal strength of three point bending σ_N^B and direct tension σ_N^T is calculated according to:

$$\sigma_N^B = \frac{3P_{\max}L}{2bD^2} = \frac{9P_{\max}}{bD} \quad \text{and} \quad \sigma_N^T = \frac{P_{\max}}{bD}$$

[16]

where P_{max} is the peak load, *L* is the length of the beam, *D* is the scaling dimension (the thickness of the beam or the width of the prism) and *b* is the depth of the beam for three point bending (40mm) or the depth of the prism (55mm) for DT specimens. Table 5.2 presents the specimens details and the mean strength value; CoV stands for coefficient of variation.

TABLE 5.1 Specimens details

Specimen ID	Replicates #	Dimensions (L x D x b)	Test Type	Average Mean Strength (MPa)	CoV %
A	12	100 x 16.7x 40 mm	Three-point bending	14.3	7.1
B	28	173 x 28.9 x 40 mm	Three-point bending	12.4	8.9
C	30	300 x 50 x 50 mm	Three-point bending	11.4	8.4
D	7	255 x 55 x 55 mm	Direct Tension	8.2	13.3

5.2 SIZE EFFECT CALCULATION

Figure 5.3 plots the resulting strength histograms on the Weibull plane (Tests Results). It is seen that the strength histogram is composed of two segments separated by a kink point, where the lower portion follows a straight line (i.e. a Weibull distribution) and the upper portion is curved, which is consistent with the finite weakest link model (see Chapter 2). The four parameters characterizing the strength cdf of the material RVE are m (Weibull modulus) and s_0, for the Weibull tail (equation 9a) and μ_G and δ_G for the Gaussian core (equation 9b). These parameters have to be linked to the five parameters of the mean size effect curve given by equation [11] and graphically expressed by figure 2.1a: N_a, N_b, r, n (scaling factor n=2 for 2D scaling for this study) and m (Weibull modulus). Weibull moduls can be obtained from the bottom right part of the experimental mean strength curve (Figure 2a) or as in this case from the low tail part of the histogram (Figure 5.3): m=26.

The remaining parameters are obtained from the experimental mean strength curve. However, since a direct tension (DT) test was used to estimate the large size domain failure behavior, the size of the DT specimen was converted into its equivalent three point bending beam according to equation [17].

$$D_{eq} = \sqrt{\frac{2(m+1)^2 N_T V_0}{6b}} = 2143 \text{ mm}$$

[17]

where D_{eq} is the equivalent characteristic beam size of the DT specimen, m is the Weibull modulus, N_T is the number of RVE in the DT specimen, V_0 is the RVE volume and b is the depth of the beam for three point bending (40mm).

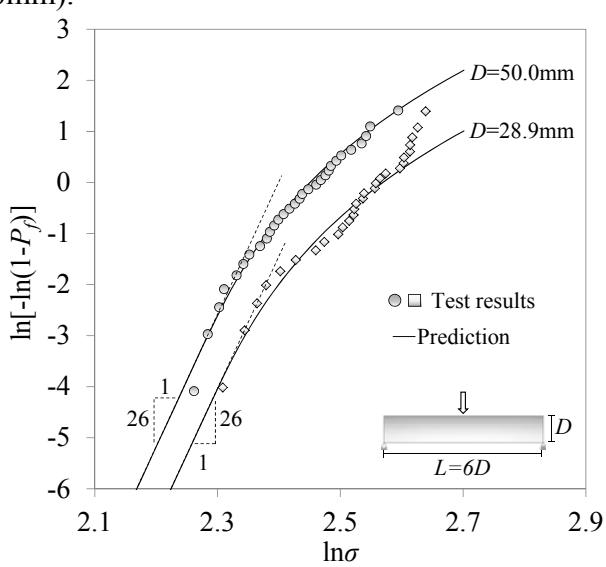

FIGURE 5.3 Asphalt mixture strength histogram

Figure 5.4 shows the mean strength curve for the strength results of Table 5.1. The curve has a typical Type I size effect pattern with and energetic-deterministic component for the small size domain and a probabilistic part governed by the Weibull statistics.

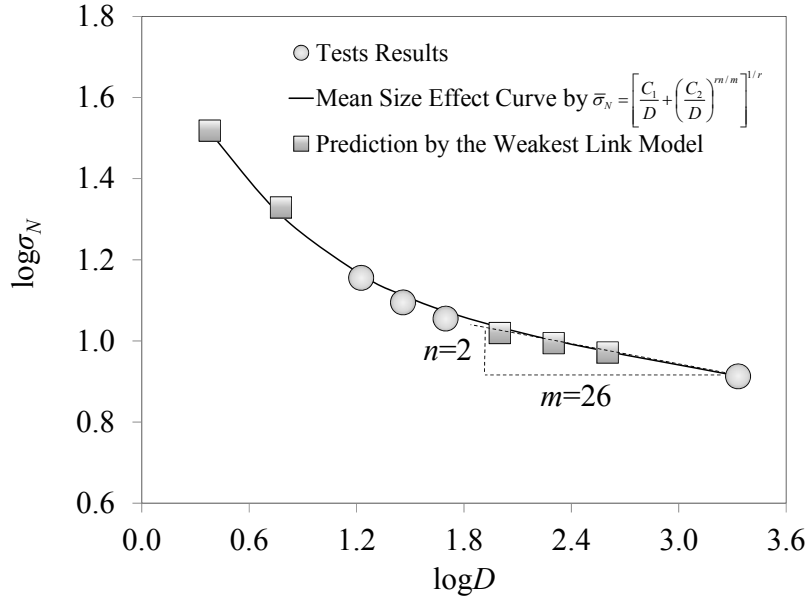

FIGURE 5.4 Mean strength size effect curve

Parameters s_0, μ_G and δ_G can then be calculated according to the following three equations for the large (equation [18]) and small (equations [19] and [20]) size domain.

$$s_0 = \left(\frac{N_b}{D_0}\right)^{n/m} \Gamma^{-1}\left(1+\frac{1}{m}\right)$$

[18]

$$\int_0^\infty \prod_{i=1}^{N} [1-P_1(s_i\sigma_N)]\mathrm{d}\sigma_N = \left[\frac{N_a}{l_m} + \left(\frac{N_b}{l_m}\right)^{rn/m}\right]^{1/r}$$

[19]

$$\frac{n}{D}\int_0^\infty \prod_{i=1}^{N} [1-P_1(s_i\sigma_N)] \sum_{i=1}^{N} \ln[1-P_1(s_i\sigma_N)]\mathrm{d}\sigma_N = -\frac{1}{r}\left[\frac{N_a}{l_m^2} + \frac{nr}{ml_m}\left(\frac{N_b}{l_m}\right)^{rn/m}\right]\left[\frac{N_a}{l_m} + \left(\frac{N_b}{l_m}\right)^{rn/m}\right]^{1/r-1}$$

[20]

where P_1 is the failure probability of the material RVE, s_i is the dimensionless stress field, σ_N is the principal stress at the center of the RVE, and D_0 can be obtained as:

$$D_0 = l_0\left[\int_V \langle s(\boldsymbol{\xi})\rangle^m \mathrm{d}V(\boldsymbol{\xi})\right]^{-1/m}$$

[21]

where ξ is the dimensionless coordinate vector.

Dimension l_m represents the smallest structure characteristic size that makes physically sense. Based on literature (*44*) the small size limit (l_m) used for solving equations [19] and [20] was set to 4RVEs. Therefore, by first fitting equation [11] to the mean strength experimental data it is possible to obtain the five parameters N_a, N_b, r, n and m. Next by using equations [18], [19] and [20], s_0, μ_G and δ_G can be calculated. For the specific asphalt mixture used in this study the following values are obtained: s_0=12.68, μ_G=45.24 and δ_G=14.82.

By knowing m, s_0, μ_G and δ_G the strength distribution of one RVE (equations [9a] and [9b]) can be calculated. With the finite weakest link model (equation [2]), it is possible to predict the strength failure distributions of beams with sizes D = 28.9 mm and D = 50 mm. Figure 5.3 shows the

comparison between the predicted (solid lines) and measured strength distribution (experimental strength histogram). It can be seen that they agree well with each other for both beam sizes B and C (Table 5.1). This verifies the values of the statistical parameters calibrated from the mean size effect curve and provides further evidence of the quasibrittleness of asphalt mixture (*21*).

Weakest link model is also used to further validate the Type I size effect behavior of asphalt mixture; the mean strength of beams with size different from those experimentally tested is predicted. It is seen from Figure 5.4 that the mean structural strength predicted from the weakest link model lies on the size effect curve represented by equation [11]. This indicates that such an expression provides a good approximation of the exact size effect curve calculated from the finite weakest link model for Type I size effect.

5.3 CONCLUSIONS

The size effect analysis confirms that asphalt mixture behaves as a quasibrittle material at low temperature showing a Type I strength size effect. The cumulative distribution function can thus be described by the grafted distribution of equations [9a] and [9b]. The dimension of RVE can be approximated, as for other quasibrittle materials such as Portland cement concrete, as two times the average aggregate size. Strength histogram and size effect theory can be used as an analysis tool also for asphalt mixture when extrapolating data to larger specimens' sizes.

CHAPTER 6

BBR ASPHALT MIXTURE STRENGTH

In this chapter asphalt mixture strength obtained with the BBR is investigated. Factors such as cooling medium, conditioning time, binder type, and the use of reclaimed asphalt material are considered in the analysis of BBR mean strength. Using size effect theory and the the results in Chapter 5, a model to describe the sub-structure of the material RVE is proposed and used to predict the strength of larger specimens.

6.1 MATERIALS AND TESTING

Table 6.1 presents the summary of the details of the five mixtures and of the experimental design used for investigating the BBR mean strength. The same three cooling media used in in Chapter 4 for asphalt binder strength study are considered: Ethanol (E) (control), Potassium Acetate (PA) and Air. Reclaimed Asphalt Mixture (RAP) is also taken into account at 20% content. Conditioning time (CT) is investigated as well at two levels: 1h (control) and 20h.

TABLE 6.1 Asphalt mixtures details and experimental design

Mixture ID	Binder	RAP	Cooling Media	Conditioning Time
Citgo	Citgo PG58-28 plain	0% (control)	E (control) – PA - Air	1h (control) – 20h
Virgin	MIF PG58-34 Elvaloy	0% (control)	E (control) – PA - Air	1h (control)
RAP	MIF PG58-34 Elvaloy	20%	E (control) – PA - Air	1h (control)
Marathon	Marathon PG58-28 plain	0% (control)	E (control) – PA - Air	1h (control) – 20h
Valero	Valero PG58-28 plain (control)	0% (control)	E (control) – PA - Air	1h (control) – 20h

All mixtures present a NMAS=12.5mm. BBR strength tests were performed on all asphalt mixture at the same temperature T=-12°C. Time to failure was set to 5 minutes as done in the size effect study of Chapter 5. BBR nominal strength was calculated according to equation [12] and the average obtained over six replicates per each testing condition.

In the second part of the experimental phase BBR strength histogram was performed in air on RAP mixture (20 replicates) and the results used predict the failure distribution of the material. The prediction is compared with a second strength histogram (28 replicates) performed on larger beams (LB) made with the same RAP asphalt mixture and tested at the same low temperature T=-12°C in air. The nominal strength on the larger beams was calculated with equation [11] using the actual dimension of the beam (125mm x 40mm x 40mm).

6.2 MEAN NOMINAL STRENGTH RESULTS

Figure 6.1 shows the mean strength obtained from BBR testing for all the factor-level combination given in Table 6.1; CoV stands for coefficient of variation (%). Figures 6.2a and 6.2b present an example of stress strain curve.

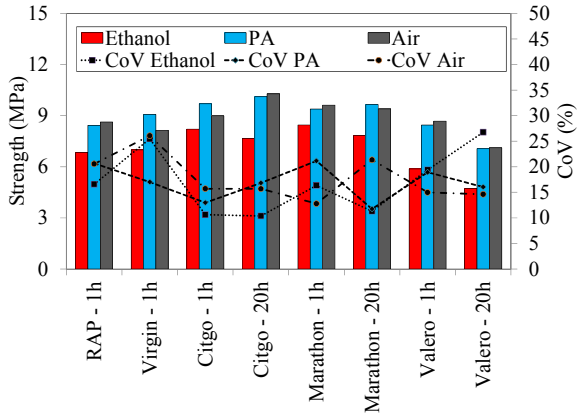

FIGURE 6.1 BBR mean strength for asphalt mixture

An increase in mixture strength is observed for tests performed in PA and air compared to those in ethanol, while similar strength values are obtained for PA and air.

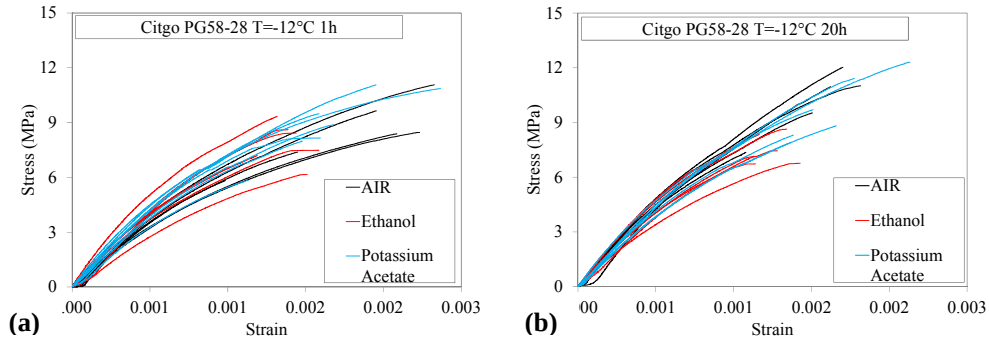

FIGURE 6.2 BBR stress-strain curve for asphalt mixture Citgo (a) 1h and (b) 20h conditioning

6.2.1 Statistical Analysis

A non-parametric statistical analysis (*41*, *42*) with an unbalanced ANOVA (*24*) is performed to determine the statistical significance of the factors assumed in the experimental design (Table 6.1).

TABLE 6.2 Statistical analysis of BBR asphalt mixture strength

Factor	Coefficients	Estimate	*t*	*p*-value
Binder Type	Citgo	1.737	4.6	**10E-8**
	MIF	1.282	4.4	**10E-8**
	Marathon	1.734	4.6	**10E-8**
	Valero	Control	-	-
Cooling Medium	Potassium Acetate	1.813	7.6	**10E-8**
	Air	1.718	7.1	**10E-8**
	Ethanol	Control	-	-

Statistical analysis shows that the response is highly binder dependent, and strongly affected by the cooling medium, with much higher values for potassium acetate and air, confirming the asphalt binder results (Chapter 4). Tukey–Kramer (*24*) multiple comparisons further provide evidence that strength results in air and potassium acetate are statistically comparable. An increase in air voids results in a decrease of the mixture strength.

6.3 RVE BUNDLE MODEL FOR BBR STRENGTH TEST

BBR strength histogram is performed on asphalt mixture RAP to evaluate the possibility of extrapolating the experimental results to larger structures. A strength histogram is obtained on larger beams (LB) made with the same mixture. Figures 6.3a and 6.3b show the two strength histograms. The two histograms clearly show a different tail of the failure probability with LB having a Weibull modulus m=28 which is exactly twice of that obtained from BBR (m=14). This suggests that the BBR beams are not fully representative of the properties of the material, and thus of the RVE.

For this reason and based on the Bundle model (*18*), a RVE mathematical model which reconstructs the RVE substructure starting from the weakest link model parameters obtained by fitting the grafted distribution of equations [9a] and [9b] to the BBR strength histogram is proposed. This model is based on two chains made of BBR sub-elements (sub-RVE of the materials derived from fitting) up to the volume of the real RVE which is estimated as twice the average aggregate grain size (6.32mm for this specific mixture having NMAS=12.5mm). Figure 6.4a shows the schematic of the RVE model. Based on equations [7] and [8] it is possible to calculate the cdf $G_2(\sigma)$ of the entire RVE. Figure 6.4b presents the failure distribution of the RVE (solid line). However, it is found that due to the limited number of chain used to raise the power tail from 14 to 28, the cdf presents a very low grafting point with a core non-Gaussian distribution part.

The model represented by equations [9a] and [9b] for the full RVE is not satisfied resulting in an over prediction of mean strength. Nevertheless, the RVE bundle model still provides the boundaries for the RVE distribution and thus, the non-Gaussian part of the cdf is approximated with a Gaussian core based on normalization condition of the entire RVE cdf. (Figure 6.4b dashed line). Therefore, it is possible to determine the four RVE parameters of equations [9a] and [9b] (m, s_0, μ_G and δ_G) and use them to predict the failure distribution of the larger beams. Figure 6.3b shows the prediction obtained with such a corrected bundle model and the weakest link model (equation [2]). The solid curve predicts very well the experimental strength data of the larger beams suggesting that the proposed approximation is a reasonable approach to the size effect analysis of strength data obtained from BBR strength tests.

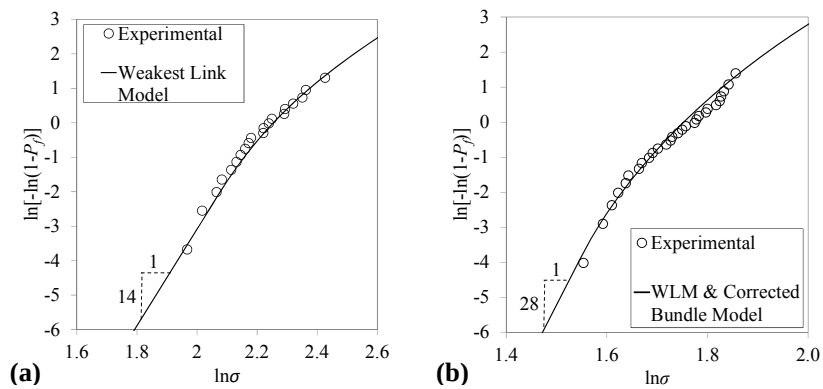

FIGURE 6.3 (a) BBR and (b) LB strength histograms for asphalt mixture RAP

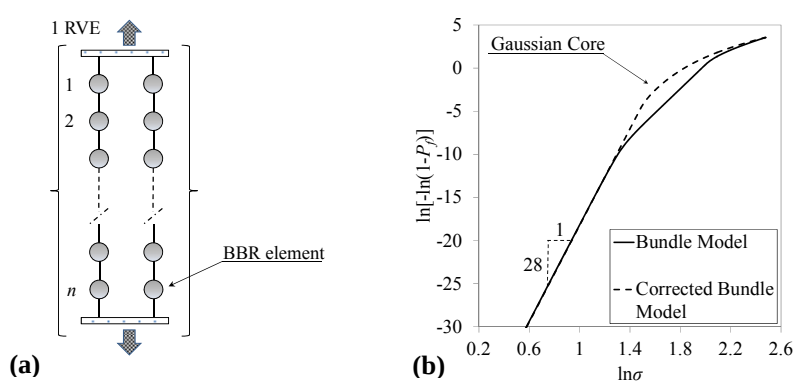

FIGURE 6.4 (a) RVE bundle model and (b) histograms of the bundle and corrected bundle model

6.4 CONCLUSIONS

Three main conclusions can be drawn from the investigation performed on BBR asphalt mixture strength. Strength obtained on small mixture beams is highly dependent on asphalt binder type and on cooling medium. The dimensions of BBR beams are not representative of the corresponding mixture RVE. This is shown by the difference in Weibull modulus between histograms obtained on BBR and much larger beams. The dimension of the actual RVE is determined by the average aggregate size. A bundle model, adjusted in the Gaussian core of the failure distribution, can be used to reconstruct the RVE starting from the fitting of the grafted cdf on the BBR experimental data. This model can be further used to extrapolate the BBR strength results to specimens of any size and geometry.

6.4.1 BBR Test Procedure for Asphalt Mixture Strength

The following steps briefly summarize the BBR strength test procedure:

- Prepare BBR beam specimens according to the procedure showed in Chapter 3, section 3.1.1;
- Condition specimens for 1h in air at the testing temperature (low PG+10°C, low PG+16°C or low PG+22°C);
- Set up the loading rate with a target failure time in the order of 5 minutes and perform tests;
- Compute nominal strength according to equation [12];
- Compute mean (average) strength (for mean strength tests);
- Plot BBR histogram (for histogram strength tests) and by using bundle and weakest link models determine the RVE parameters; convert BBR strength to direct tension strength through weakest link model.

CHAPTER 7

ASPHALT BINDER AND MIXTURE BBR CREEP

The investigation of asphalt binder and asphalt mixture BBR strength showed a significant effect of the cooling medium on the measured values or the response. In this chapter a simple study on the possible influence of the cooling medium on asphalt binder and asphalt mixture creep is presented.

7.1 MATERIALS AND TESTING

The same asphalt binders and same asphalt mixtures used in Chapter 6 are selected for the experimental phase. One single testing temperature is used and set to low PG+10°C. Testing procedures and creep stiffness and *m*-value calculation are performed according to the current AASHTO standard (*1*) for asphalt binder and following the method proposed by Marasteanu et al. (*33*) for asphalt mixture. Test duration was set to 1000s. Tables 7.1 and 7.2 present materials details and experimental design.

TABLE 7.1 Asphalt binder details and experimental design

Binder	Aging	Cooling Media	Conditioning Time
Citgo PG58-28 plain	RTFOT – PAV (control)	E (control) – PA - Air	1h (control) – 20h
MIF PG58-34 Elvaloy	RTFOT – PAV (control)	E (control) – PA - Air	1h (control) – 20h
Marathon PG58-28 plain	RTFOT – PAV (control)	E (control) – PA - Air	1h (control)
Valero PG58-28 plain (control)	RTFOT – PAV (control)	E (control) – PA - Air	1h (control)

TABLE 7.2 Asphalt mixtures details and experimental design

Mixture ID	Binder	RAP	Cooling Media	Conditioning Time
Citgo	Citgo PG58-28 plain	0% (control)	E (control) – PA - Air	1h (control)
Virgin	MIF PG58-34 Elvaloy	0% (control)	E (control) – PA - Air	1h (control) – 20h
RAP	MIF PG58-34 Elvaloy	20%	E (control) – PA - Air	1h (control) – 20h
Marathon	Marathon PG58-28 plain	0% (control)	E (control) – PA - Air	1h (control)
Valero	Valero PG58-28 plain (control)	0% (control)	E (control) – PA - Air	1h (control)

7.2 RESULTS AND STATISTICAL ANALYSIS

Figures 7.1a and 7.1b show the average (Av) creep stiffness curves for Citgo and MIF asphalt binders, while Table 7.3a and 7.3b present the results of the statistical analysis (ANOVA) for creep stiffness and *m*-value at t=60s: *S*(60) and *m*(60).

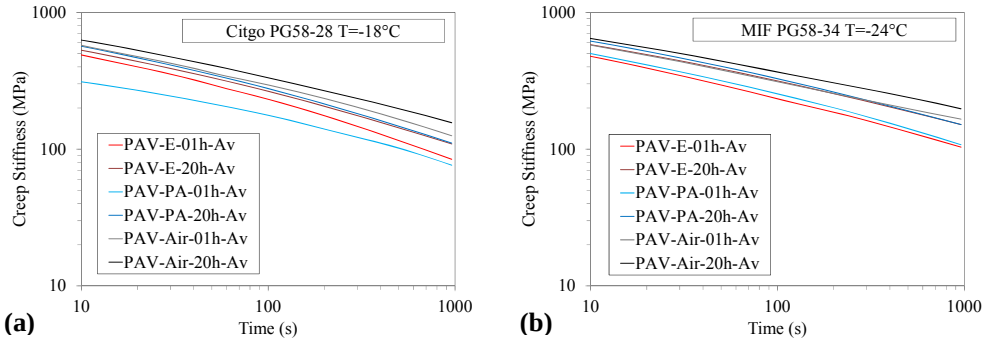

FIGURE 7.1 BBR creep stiffness curves for asphalt binder (a) Citgo PG58-25 and (b) MIF PG58-34

All factors are significant both for *S*(60) and *m*(60). Tukey–Kramer (*24*) multiple comparisons clearly shows that specimens tested in air presents higher stiffness compared to those in ethanol and potassium acetate. An interaction between cooling medium and aging is also significant with increasing stiffness results for PAV condition. Higher stiffness values are obtained for asphalt binder MIF with a clear distinction between all the four binders used. Statistical interaction between conditioning time cooling medium is detected for *m*(60). Higher relaxation capabilities are obtained for tests in ethanol and air (which are statistically similar) compared to potassium acetate.

TABLE 7.3 ANOVA *F* tests results of asphalt binder for *S*(60) and *m*(60)

Source - S(60s)	***F***	***p*-value**
Binder Type	489.6	**1E-08**
Cooling Medium	114.7	**1E-08**
Conditioning Time	92.9	**1E-08**
Aging	338.8	**1E-08**
Cooling Medium.Aging	4.8	**0.011**

Source - m(60s)	***F***	***p*-value**
Binder Type	123.9	**1E-08**
Cooling Medium	242.7	**1E-08**
Conditioning Time	136.8	**1E-08**
Aging	836.7	**1E-08**
Conditioning Time.Cooling Medium	3.8	**0.029**

Figures 7.2a and 7.2b present the average (Av) creep stiffness curves for Citgo and RAP asphalt mixtures, while Table 7.4a and 7.4b show the output of the ANOVA *F*-test for creep stiffness and *m*-value at t=60s: *S*(60) and *m*(60).

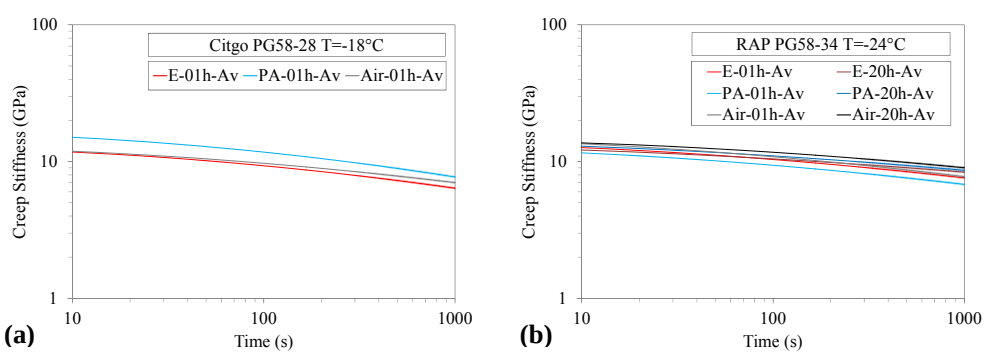

FIGURE 7.2 BBR creep stiffness curves for asphalt mixtures (a) Citgo and (b) RAP

TABLE 7.4 ANOVA *F* tests results of asphalt binder for *S*(60) and *m*(60)

Source - S(60s)	***F***	***p*-value**
Binder Type	1215.2	**1E-08**

Source - m(60s)	***F***	***p*-value**
Air Voids	5.7	**1E-08**
Binder Type	13.7	**1E-08**
Conditioning Time	44.8	**0.028**

A much simpler behavior is found for asphalt mixture creep stiffness that is statistically affected only by binder. MIF, Citgo and Marathon provide comparable *S*(60), while lower values are found for Valero. *m*(60) presents a much more complex behavior. Air voids content strongly affects the relaxation properties of the mixture. Binder type and cooling time are also significant. It is very interesting to notice there is no cooling medium effect both for *S*(60) and *m*(60).

7.3. CONCLUSIONS

A number of general conclusions can be drawn from this brief investigation on asphalt binder and asphalt mixture creep stiffness. Cooling medium highly affects asphalt binder creep stiffness and relaxation capabilities. Air is responsible for an increase in stiffness, while potassium acetate lowers the *m*-value. In the case of asphalt mixture no cooling medium effect is detected, while an increase in air voids clearly increases the relaxation properties of the mixture. Overall a complex behavior of both asphalt binders and mixture is detected.

CHAPTER 8

CONCLUSIONS, PLANS FOR IMPLEMENTATION, AND RECOMMENDATIONS FOR FURTHER RESEARCH

8.1. CONCLUSIONS

The idea of performing strength tests on asphalt binder and asphalt mixture beam specimens with the Bending Beam Rheometer (BBR) at low temperature was investigated in this project. The BBR has many advantages over the current DTT and IDT specifications: most asphalt testing laboratories have the BRR, only a modification of the loading frame is needed to perform load controlled strength tests, calibration is very simple, and testing smaller size specimens make possible investigating the properties of thin layers of asphalt mixtures at different depths in the pavement. The three-point bending configuration also allows for extrapolation of strength results to larger structures and different stress fields.

For asphalt mixtures, from the statistical analysis of BBR strength results, a significant effect was observed with temperature, mixture type, loading rate and air void content. Comparison of the BBR strength and IDT strength indicated a statistically significant difference between the two methods, with much higher strength values for BBR. This is most likely due to differences in stress field in the two specimens and the complex size dependence of the IDT strength.

For asphalt binders, from the statistical analysis of BBR strength results, it was observed that DTT strength measured in potassium acetate was much higher than BBR strength measured in ethanol. However, when BBR strength tests were run in the same cooling medium, the BBR loading rate was set to match the DTT time to failure, and Weibull size effect theory was used to take into account the different size and stress field of the DTT and BBR specimens, is was found that BBR and DDT strength results are comparable.

To address the cooling medium issue in asphalt binders, BBR strength tests were performed using three different cooling media: ethanol, potassium acetate and air. Statistical analysis confirmed the previous findings and showed that testing in potassium acetate and in air results in similar strength values. BBR strength in air and DTT strength in potassium acetate were compared through histogram testing and similar mean values were found using the weakest link model and the RVE grafted cdf. This suggests the weakest link model can be used as an analysis tool of the BBR binder strength obtained in air when a sufficiently short time to failure (15-20s) is used to limit a dominant viscoelastic behavior of the binder.

Experimental results and size effect modeling showed that asphalt mixtures have a type I strength size effect and confirmed the quasibrittle behavior at low temperature. Based on histogram experimental data, it was found that the grafted failure distribution of the RVE is a reasonable model assumption for asphalt mixtures; RVE size was estimated as twice of the average grain size of the aggregate phase. The issue of uniaxial tensile strength versus flexural strength was also addressed by performing asphalt mixture direct tension tests. For sufficiently large specimens, it was found that simple Weibull statistics can be used to convert one stress field into another, and vice versa. Based on these results, strength histogram can be adopted as an analysis tool for asphalt mixture strength as well.

Non-parametric statistical analysis of the mean asphalt mixture strength results indicated that binder type and cooling medium were significant, with air and potassium acetate giving similar results. It was also found that BBR asphalt mixture beams are not sufficiently large to be representative of the real dimension of the RVE. As a consequence, a bundle model was used to reconstruct the RVE sub-structure of the material. Based on this model and on weakest link model, the BBR results were compared with the strength histogram obtained on larger asphalt mixture beams; it was determined that the proposed bundle, model adjusted in the Gaussian core, can be used to extrapolate the BBR data to larger structures.

A short investigation on the effect of cooling medium on asphalt binder and asphalt mixture creep was also performed. For asphalt binders, it was found that creep stiffness and relaxation properties are highly affected by cooling medium: testing in air results in higher stiffness, while potassium acetate leads to lower *m*-values. For asphalt mixtures, no cooling medium effect was detected, which validates the test method proposed in a previous Idea project.

From the experimental work and statistical modeling it can be concluded that strength tests can be performed on asphalt binders and asphalt mixtures with the modified BBR. Cooling in air appears to be the best option for storing and testing both binders and mixtures. Size effect theory can then be used to manipulate and extrapolate experimental data to stress field that are independent of the specific specimen size and geometry used.

8.2. PLANS FOR IMPLEMENTATION

The research performed in this project was presented at national and international meetings and has received considerable attention over the past year. The PI has also made presentations at the two asphalt mixture ETG meetings in 2012. It is expected that, based on input from panel members and the asphalt community, a draft specification for obtaining low temperature bending strength for asphalt binders and asphalt mixtures using the BBR will be developed and will be presented at the upcoming asphalt mixture ETG meetings for discussion and approval before submitting it to AASHTO.

8.3. RECOMMENDATIONS FOR FURTHER RESEARCH

The results obtained in this investigation indicate that the BBR system can be used to obtain strength properties of asphalt binder and mixtures. Two important issues need to be further addressed until full implementation of these methods is achieved. The experimental results and analyses indicated that using air as a cooling medium would eliminate any concerns related to the effect of cooling fluid on asphalt material properties. However, controlling air temperature in

the BBR cooling chamber is challenging. While in this research effort extreme care was taken to control the temperature, this may be difficult to achieve on a routine basis. Secondly, some of the mixture specimens tested had strength values in air that exceeded the limits of the load cell. This needs to be further investigated since it may require retrofitting the BBR with a larger load cell.

REFERENCES

1. American Association of State Highway and Transportation Officials (AASHTO). Standard T313-10-UL, *Standard Method of Test for Determining the Flexural Creep Stiffness of Asphalt Binder Using the Bending Beam Rheometer (BBR)*. 2010.
2. American Association of State Highway and Transportation Officials (AASHTO). Standard T314-07-UL, *Standard Method of Test for Determining the Fracture Properties of Asphalt Binder in Direct Tension (DT)*. 2007.
3. American Association of State Highway and Transportation Officials (AASHTO). Standard T322-07-UL. *Standard Method of Test Determining the Creep Compliance and Strength of Hot-Mix Asphalt (HMA) Using the Indirect Tensile Test Device*. 2007.
4. M. Marasteanu, R. Velasquez, A. Zofka and A. Cannone Falchetto. *Development of a Simple Test to Determine the Low Temperature Creep Compliance of Asphalt Mixture. IDEA Program Final Report NCHRP 133*, July 2009.
5. L. da Vinci. Discorsi e Dimostrazioni Matematiche intorno a Due Nuove Scienze. Elsevirii Leiden, English transaltion by T. Weston, London, 1730, pp. 178-181.
6. E. Mariotte. *Traité du Mouvement des Eaux*. Posthumously edited by J.T. Desvaguliers London, 1918.
7. M. Fréchet. Sur la Loi de Probabilité de l'Écart Maximum. Annales Societatis Mathematicae Polonae, Vol. 6, 1927, pp. 93–116.
8. W. Weibull. The Phenomenon of Rupture in Solids. Proceedings of Royal Swedish Institute of Engineering Research, Vol. 151, Stockholm, 1939, pp. 1–45.
9. Z. P. Bažant. *Scaling of Structural Strength*. Elsevier, London, 2005.
10. R. H. Leicester. The Size Effect of Notches. Proceedings of the 2nd Australian Conference of Mechanics of structures and Materials, Melbourne, 1969, pp. 4.1–4.20.
11. A. Hilleborg, M. Modéer and P. E. Petersson. Analysis of Crack Formation and Crack Growth in Concrete by Means of Fracture mechanics and Finite Elements. Cement and Concrete Research, Vol. 6, 1976, pp. 773-782.
12. A. Carpinteri and B. Chiaia. Fracture Mechanics of Concrete Structures. Proceedings of FraMCoS-2, Wittmann FH, Aedificatio Publisher, Freiburg, 1995, pp. 581-596.
13. Z. P. Bažant and D. Novák. Energetic-Statistical Size Effect in Quasibrittle Failure at Crack Initiation. ACI Materials Journal, Vol. 97(3), 2000, pp. 381–392.
14. Z. P. Bažant and S.-D. Pang. Activation Energy Based Extreme Value Statistics and Size Effect in Brittle and Quasibrittle Fracture. Journal of Mechanics and Physics of Solids, Vol. 55, 2007, pp. 91–134.
15. Z. P. Bažant, J-L. Le and M. Z. Bažant. Scaling of Strength and Lifetime Distributions of Quasibrittle Structures Based on Atomistic Fracture Mechanics. Proceedings of the National Academy of Science USA, Vol. 106, 2009, pp. 11484-11489.
16. J-L. Le, Z. P. Bažant and M. Z. Bažant. Unified Nano-Mechanics Based Probabilistic Theory of Quasibrittle and Brittle Structures: I. Strength, Static Crack Growth, Lifetime and Scaling. Journal of Mechanics and Physics of Solids, Vol. 59, 2011, pp. 1291–1321.
17. Z. P. Bažant and J. Planas. *Fracture and Size Effect in Concrete and Other Quasibrittle Materials*. CRC Press, 1998.
18. E. Daniels. The Statistical Theory of the strength of Bundles and Threads. Proceedings of the Royal Society A, Vol. 183, 1945, pp. 405–435.
19. E. Johnson, T. Clyne and B. Worel. *MnROAD Phase II Construction Report*. Minnesota Department of Transportation, 2009.
20. T. Clyne and L. Palek. *Low Volume Road & Farm Loop Cells 33, 34, 35, 77, 78, 79, 83, 84 Construction Report*. Minnesota Department of Transportation, 2008.
21. M. Turos, A. Cannone Falchetto, G. Tebaldi and M. O. Marasteanu. Determining the Flexural Strength of Asphalt Mixtures Using the Bending Beam Rheometer. Proceeding of the 7th RILEM Conference on Cracking in Pavements, (in press)
22. H. Rinne. *The Weibull Distribution. A Handbook*. CRC Press, 2009.
23. MATLAB. Help documentation, R2008a, 2008.
24. G. W. Oehlert. *A First Course in Desing and Analysis of Experiments*. W. H. Freeman, 2000.
25. D. W. Christensen and R. F. Bonaquist. *Evaluation of Indirect Tensile Test (IDT) Procedures for Low-Temperature Performance of Hot Mix Asphalt*. NCHRP Report 530, Washington, D.C., Transportation Research Board, 2004.
26. G. M. Sabnis and S. M. Mirza. Size Effects in Model Concretes. Journal of the Structural Division. Vol. 105(6), 1979, pp. 1007-1020.
27. J-K. Kim. *Size Effect on the Splitting Tensile Strength of Concrete and Mortar*. Report No. CM 89-3, Korea Advanced Institute of Science and Technology, 1989, Seoul.
28. W-F. Chen and R. L. Yuan. Tensile Strength of Concrete: Double Punch Test. Journal of the Structural Division, Vol. 106, 1980, pp. 1673-1693.

29. T. Hasegawa, T. Shioya and T. Okada. Size Effect on Splitting Tensile Strength of Concrete. Proceeding of Japan Concrete Institute 7th Conference, 1985, pp.309-312.
30. C. Rocco, G. V. Guinea, J. Planas and M. Elices. The Effect of Boundary Conditions on the Cylinder Splitting Strength. Fracture Mechnaics of Concrete Structures. F. H. Wittmann edition, Freiburg , Germany, 1995, pp.75-84.
31. Z. P. Bažant, S. He, M. E. Plesha and R. E. Rowlands. Rate Size Effects in Concrete Fracture: Implication for Dams. Proceedings of the International Conference on Dam Fracture, V. Saouma, R. Dungar and D. Morris editions, University of Colorado, Boulder, Colorado, 1991 pp. 255-261.
32. C. Rocco. Influencia del Tamaño y Mecanismos de Rotura del Ensayo de Compresion Diametral. Doctoral Thesis, Dep. Ciencia de Materiales, Universidad Politecnica de Madrid, Madrid, Spain, 1996.
33. M. O. Marasteanu, A. Zofka, M. Turos, X. Li, R. Velasquez, X. Li, W. Buttlar, G. Paulino, A. Braham, E. Dave, J. Ojo, H. Bahia, C. Williams, J. Bausano, A. Kvasnak, A. Gallistel and J. McGraw. *Investigation of Low Temperature Cracking in Asphalt Pavements (National Pooled Fund Study 776 Final Report)*. Minnesota Department of Transportation.
34. American Association of State Highway and Transportation Officials (AASHTO). Standard T240-09-UL, *Test for Effect of Heat and Air on a Moving Film of Asphalt (Rolling Thin-Film Oven Test)*. 2009.
35. American Association of State Highway and Transportation Officials (AASHTO). Standard R028-09-UL, *Standard Practice for Accelerated Aging of Asphalt Binder Using a Pressurized Aging Vessel (PAV)*. 2009.
36. S. E. Swartz and H. C. Siew. Is Load Control Suitable for Fracture-Energy Measurements for Concrete? Experimental Mechanics, Vol. 27(4), 1987, pp. 359-365.
37. J. Dongré and J. D'Angelo. Effect of New Direct Tension Test Protocol on the Superpave Low-Temperature Specification for Bitumen Binders. Bearing Capacity of Roads and Airfields, 1998.
38. R. A. Rubeck. Kinetics of Environmental Stress Cracking in High Density Polyethylene. Polymer, Vol. 22(5), 1981, pp. 682-686.
39. J. C. Arnold. The Influence of Liquid Uptake on Environmental Cracking of Glassy Polymers. Materials Science and Engineering A, Vol. 197, 1995, pp. 119-124.
40. E. J. Moskala. A Fracture Mechanics Approach to Environmental Stress Cracking in Poly(ethyleneterephtalate). Polymer, Vol. 39(3), 1998, pp. 675-680.
41. D. S. Moore, G. P. McCabe and B. A. Craig. *Introduction to the Practice of Statistics*. W. H. Freeman and Company, New York, 2009.
42. R. D. Cook and S. Weisberg. *Applied Regression Including Computing and Graphics*. A Wiley-Interscience publication, 1999.
43. D. Lesuer. The colloidal Structure of Bitumen: Consequences on the Rheology and on the Mechanics of Bitumen Modification. Advances in Colloid and Interface Science, Vol. 145, 2009, pp. 42-82.
44. J-L. Le, J. Eliáš and Z. P. Bažant. Computation of Probability Distribution of Strength of Quasibrittle Structures Failing at Macro-Crack Initiation. Journal of Engineering Mechanics, ASCE, 2012 (in press).